United States Department of the Interior

U. S. Geological Survey

THERMAL CONDUCTIVITY OF ROCKS

by Eugene C. Robertson

1979

Open File Report 79-356

THERMAL CONDUCTIVITIES OF ROCKS

by Eugene C. Robertson
U.S. Geological Survey
Reston, Virginia 22092

Introduction

A mathematical model of a physical property of a rock would be most satisfactory for explanation and prediction if based on a physical model incorporating the chemical and physical properties of the pure components of the rock, including the minerals and fluids composing the rock. The calculation of some scalar properties of rocks is easily done (e.g. density and specific heat), but vector properties of second order, e.g. most thermal properties, require more complicated models for calculation from pure mineral properties because of the effects of texture and anisotropy. This present compilation of thermal properties is primarily empirical, not theoretical, due to insufficient data on composition, pore characteristics, and temperature effects. The principal objective of preparing the graphs of this report is to provide a means of estimating thermal conductivity for practical purposes, that is, estimation of conductivity of a rock from a few of its characteristics. It is anticipated that conductivity estimates from the graphs for inaccessible or unmeasurable rocks, and of course as a time-saver, will be useful for radioactive waste, heat flow, and geothermal resource appraisals.

Analysis of measurements of the thermal conductivity of rocks made at about 35°C (300K) and 50 bars (5MPa) reveals that the effects of porosity, water content, and quartz or olivine content can be combined in a single plot for purposes of estimating the conductivity. Graphs have been prepared for the principal rock types, in the belief that line drawings provide more immediately understood information than tables do, and with the purpose of showing how well the data support the lines drawn. Each figure is described separately herein, and the intercepts of the lines are given so that interpolated values can be calculated. By showing the quartz or olivine data on the plots, an estimate of uncertainty can be made. The important temperature effect on conductivity is shown on a separate set of drawings.

These figures are empirical and are based on the available data in the literature. The approach is that developed as a result of a thorough study of the conductivity of vesicular basalt by Robertson and Peck (1974), one innovative result of which was the finding of a relation between conductivity and solidity.

Solidity

The parameter used here to account for the insulating effect of pore spaces on conductivity is called solidity. Solidity, γ, is defined as the ratio of the volume of solid to the bulk volume, which equals the ratio of bulk density to solid grain density; it is the complement of porosity, ϕ, i. e., $\gamma = 1 - \phi$. Robertson and Peck (1974) found that the thermal conductivity of basalt varies linearly as the square of the solidity, γ^2.

The effect of the pore spaces on resistivity of rock is given by Archie's Law, in which resistivity of the rock varies inversely as the square of porosity; this result was corroborated by a resistor network study by Greenberg and Brace (1969); the electrical conduction is apparently controlled primarily by the electrolyte in the connected pores. In a similar way, thermal conduction in a rock is apparently controlled by solid grain-to-grain paths. Adler et al (1973) used an experimental resistor simulation to show that the bulk electrical conductivity of a three-dimensional lattice is proportional to the square of the fraction of conducting bonds, and thus they provide a theoretical model for Archie's Law and by analogy provide a theoretical thermal conduction model for the K vs γ^2 relationship. Other physical and mathematical models do not fit the experimental results on basalt as well (see Robertson and Peck, 1974). This conclusion is born out by analysis of the results of Hutt and Berg (1968) and other investigators for sandstone, shown in Figure 9, and of the results for limestone (Figs. 4 and 5) and for dolomite (Fig. 6) from various sources.

A possible confusion may occur in distinguishing between the symbols, italic K for conductivity and Roman K for Kelvins, the SI unit of temperature. The usage and the italic underline should prevent ambiguity.

Pore Fluid

The influence on $\underline{K}$ of the fluid in the rock pores is quite important. The enhancement of $\underline{K}$ by saturation with water compared to air is shown in the pairs of Figures 1 and 2, 4 and 5, and 8 and 9. (Although there are some data available for the effects on $\underline{K}$ by various gases and hydrocarbon fluids in the pores, only a few rocks have been studied, so no attempt is made to show them here.) The values of $\underline{K}$ for dry samples with air in the pores and those for saturated samples with water in the pores are shown by separate plots for each of the principal rock types (except felsic and ultramafic rocks), in Figure 1 to 13.

In the earth, most rocks are fully saturated with water below the water table, which occurs generally at depths shallower than 30 m. For certain purposes, however, partial saturation must be considered. The increase in $\underline{K}$ with increasing water saturation is actually quite variable, depending on rock type and fluid permeability. However, a rough linear approximation can be adduced, based on very sparse data, to interpolate between values from the air-saturated and the water-saturated plots: for many rocks, at a given $\underline{\gamma}$, about 80 percent of the increase in $\underline{K}$ due to addition of water in the pores is attained at about 50 percent saturation; linear interpolations can be made to the air-saturated and to the water-saturated values of $\underline{K}$ from this point, constituting the locus from which to estimate $\underline{K}$.

In Figures 1 and 2 for basalt, the extrapolated intercept at the left at $\underline{\gamma} = 0$ is higher than the values of $\underline{K}$ for air and for water, respectively; a less well-defined higher intercept at $\underline{\gamma} = 0$ is shown for felsic rocks in Figure 3. The explanation for lack of correspondence may be that at low $\underline{\gamma}$ the thin web of rock grains around the pores conducts heat more efficiently than the pore air or water and thus perturbs a strict $\underline{\gamma}^2$ volumetric variation for $\underline{K}$. In Figures 4 to 13, for the other rocks, the intercepts are fixed at the air and water values of $\underline{K}$, due to lack of data at low $\underline{\gamma}$.

Quartz, Olivine, and Clay Content

In their study of basalt, Robertson and Peck (1974) found that $\underline{K}$ increases systematically with increase in content of olivine phenocrysts

in the samples (isopleths in Figs. 1 and 2). The ground mass of the rock is fine-grained (about .03 mm dia), augite and labradorite mostly, and its $\underline{K}$ apparently varies quite uniformly over a wide range of γ. It was concluded that the $\underline{K}$ of a tholeiitic basalt could be well estimated from knowledge of its γ, water content, and proportion of olivine phenocrysts. Also in that paper, it was found that the $\underline{K}$ of basalt can be estimated from the mineral and pore composition using correction factors for the intercepts; however, no effort is made herein to discuss this more basic approach.

An even more important mineral affecting rock conductivity is quartz. At 35° C and 50 bars, average $\underline{K}$ of quartz is about 18×10^{-3} cal/cm sec deg C; this value of $\underline{K}$ is 3 times that of the massive granite and 4 times that of dense basalt. The effect of quartz content was ascertained in large part from mineral compositions and conductivities of a suite of sandstones from measurements made by Hutt and Berg (1968); Figures 8 and 9 were also derived from modal and conductivity observations of Woodside and Messmer (1961), Zierfuss and Vliet (1956), and Clark (1941), with supporting data from other sources, as described for Figures 8 and 9 below.

The graphs for sandstone (Figs. 8 and 9) provided the bases for making sense of the available data for $\underline{K}$ of shale and soils. Only 2 studies of shales included mineral compositions, but several studies of soils did include such information, and fortunately the water-saturated data for soils fits reasonably well with the sandstone and usable shale data. Air-saturated soils are very different, as described for Figure 12 below.

The plot (Fig. 3) for felsic igneous rocks is poorly substantiated, as there is almost no data available for the effect of γ. The correlation of $\underline{K}$ with estimated quartz content in the porous rocks is very rough, also. However, as described for Figure 3, the graphs for sandstone, Figures 8 and 9, can be used for porous felsic igneous rocks, probably without large error. Values of $\underline{K}$ for dense felsic rocks ($\gamma > .95$) are plentiful, and fairly reliable and methods of calculating $\underline{K}$ from their rock modes have been discussed by Birch and Clark (1940) and Beck and Beck (1958).

Clay minerals, like montmorillonite, illite, and kaolin, are found in shaley rocks, and their presence lowers the thermal conductivity. This lowering is due to the low conductivity normal to the clay flakes, about 1 CU, compared to 8 CU parallel to the flake layers. The $\underline{K}$ is reduced also by the presence of air-filled pore space between flakes, which is usually very, very small, less than the mean free path of air molecules. The decrease in $\underline{K}$ by the presence of clay minerals is opposite to the increase due to quartz content, discussed under Figures 10, 11, and 12, for shales and soils.

The extrapolated intercept of the isopleths at $\gamma^2 = 1$, the fully solid condition, is not necessarily the intrinsic value calculated from single crystal mineral conductivities. In fact, the results of Robertson and Peck (1974) on basalt show an intercept well below the calculated and measured average of mineral $\underline{K}$'s. The effective $\underline{K}$ is 15 percent below the intrinsic $\underline{K}$ for water-saturated basalt in samples of $.995 < \gamma < 1$, due to the insulating effect of thin air-filled pores, minute vesicles, and microfractures created by cooling stresses.

Temperature Effect

There is a drastic decrease in $\underline{K}$ with increasing temperature $\underline{T}$ for quartz and halite (Figs. 20 and 21), and the principal rock types except basalt also show decrease in $\underline{K}$ with increase in $\underline{T}$, as shown in Figures 15 to 18. Basalt shows a small rise in $\underline{K}$ with $\underline{T}$ (Fig. 14). Glasses also have a positive $\underline{T}$ effect, (Fig. 19), but this is not surprising, as glasses are anomalous in other of their physical properties (e.g. elastic).

The graphs of the $\underline{T}$ effect can be utilized by taking a $\underline{T}$ curve for a rock sample with known (or estimated) $\underline{K}$ at 35° C and following the curve to the $\underline{T}$ of interest.

Description of Figures

Introduction

Each of the Figures from 1 to 21 is described individually below, giving references to sources of data, and explaining use of symbols, numbers on the plots, intercepts, and other matters to be emphasized. In Figures 1 to 13, $\underline{K}$ is plotted against γ^2, and isopleths show variation with olivine or quartz content. As can be seen, the values alongside the plotted points do not define the locations of the isopleths exactly; such secondary effects on $\underline{K}$ as anisotropy and variation in composition and texture affect the grain-to-grain thermal coupling of the matrix of the rock samples and account for the lack of correspondence.

Intercepts will be given for easy calculation of interpolated values; a formula like the following can be used:

$$\underline{K} = \underline{K}_F + \underline{\gamma}^2 [K_S + p\,C) - K_F] \qquad (1)$$

where $\underline{K}_F$ is pore fluid intercept at $\underline{\gamma}^2 = 0$, $\underline{K}_S$ is solid rock intercept at $\underline{\gamma}^2 = 1$, for zero percent quartz or olivine, p is percent quartz or olivine, and C is a constant equal to the change of $\underline{K}$ with quartz or olivine per unit percent, obtained from the intercept values at $\underline{\gamma}^2 = 1$ on the figures. The value of solidity $\underline{\gamma}$ can be obtained from the relation with porosity $\underline{\phi}$, $\underline{\gamma} = 1 - \underline{\phi}$, and from ratio $\underline{\gamma} = \underline{d}_B / \underline{d}_G$, where $\underline{d}_B$ is bulk density, and $\underline{d}_G$ is grain density. By laboratory measurements, $\underline{\gamma}$ can be obtained from the weight of a sample dry $\underline{W}_D$ and the weights saturated with water in air $\underline{W}_{WA}$, and immersed in water, $\underline{W}_{WW}$, as follows: $\underline{\gamma} = (\underline{W}_{WA} - \underline{W}_D) / (\underline{W}_{WA} - \underline{W}_{WW})$.

No precision or accuracy values are given herein because the graphs are preliminary and need corroboration. Visual estimates from the scatter of point values can be taken as a measure of the uncertainty in estimating values. No statistical calculations have been made on the data in any drawing to compare observed $\underline{K}$ with calculated $\underline{K}$.

Both SI and cgs units are shown in the figures, and the conversion factor for thermal conductivity is: $1\,W/mK = 2.390 \times 10^{-3}$ cal/cm sec deg C. The acronym CU will be used for conductivity unit $= 10^{-3}$ cal/cm sec deg C.

Figure 1.

The points plotted in this figure are data from Robertson and Peck (1974) on tholeiitic basalt samples, dry, with air in the pores. The quadratic relation of the axes of their Figure 7 has been changed from $\sqrt{K}$ vs γ to K vs γ^2 to make the charts easier to use. The olivine content of the samples is shown adjacent to each point, and the scatter of values with respect to the isopleth lines is clear. Given the uncertainty of estimating K from γ and the water and modal olivine contents, the following intercepts apply for purposes of calculation in equation 1.

γ	Olivine (Vol. %)	K (CU)
0	0	0.45
1	0	3.60
1	30	4.68

The control of points is good enough to place the intercepts (0.45 CU), at $\gamma = 0$, higher than the actual air value (0.063 CU), and the intercept (3.78 CU), at $\gamma = 1$ for 5 percent olivine, lower than the calculated value (6.10 CU). The isopleth lines have been drawn radially to a single point (0.45 CU), at $\gamma = 0$, as a better fit than a set of parallel lines, which would give the next easiest arrangement for calculation purposes.

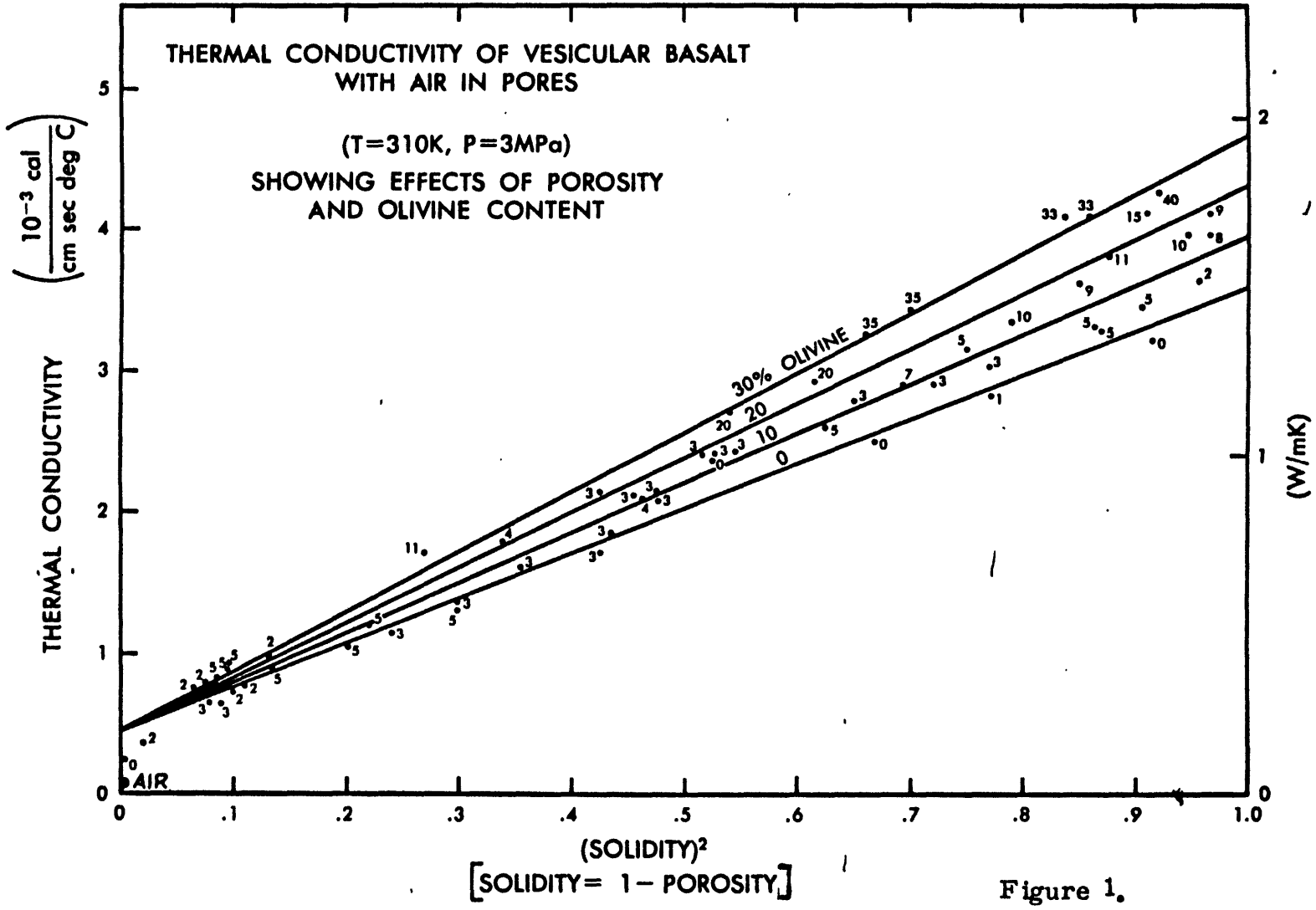

Figure 1.
(Robertson)

7a

Figure 2.

The points in this figure are from observed data of Robertson and Peck (1974), on conductivity of water-saturated basalt, with revised axes from their Figure 8. The isopleth lines are shifted upward by the improved thermal conduction through the water compared to air (Fig. 1). The following intercepts can be used in calculating K.

γ	Olivine (Vol %)	K (CU)
0	0	1.80
1	0	4.40
1	30	6.20

As in Figure 1, the intercept at $\gamma = 0$, is 1.80 CU, higher than the water value, $K = 1.48$; at $\gamma = 1$, the intercept for basalt with 5 percent olivine is 4.70 CU, whereas the calculated and observed pure-mineral average is 6.10 CU. The radial pattern of isopleths of equal olivine content is somewhat forced, but this arrangement fits the data points better than a parallel one, as in Figure 1.

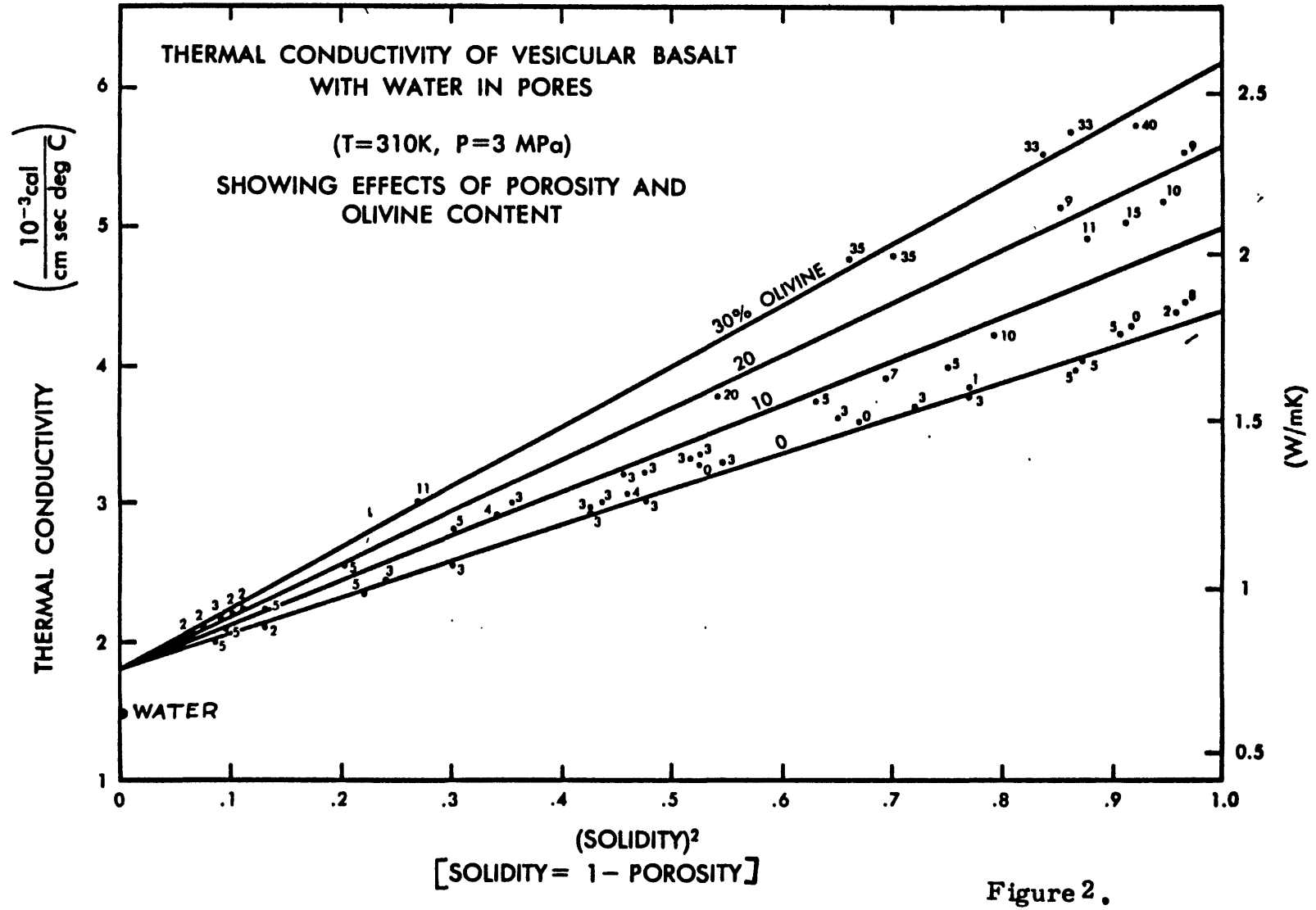

Figure 2.
(Robertson)

Figure 3.

The data on dense ($\gamma > 0.95$) felsic igneous rock, air saturated, shown in this figure, are merely representative of hundreds of measurements made on such rocks. The upper quartz monzonite and obsidian points shown are from Birch and Clark (1940); they describe ways of calculating $\underline{K}$ from felsic rock modes, as do Beck and Beck (1958). The other data plotted (Fig. 3), for $\gamma < 0.9$, are from Gordon Green (written communication, 1966); most of the points are averages of 2 to 9 measurements, and the data at low solidity, $\gamma < 0.6$, are the only ones available at the present time. The quartz contents were estimated, not observed. No data are available on water-saturated felsic igneous rocks at low _ .

The intercepts are tabulated below.

γ	Quartz (Vol %)	$\underline{K}$ (CU)
0	0	0.45
1	0	2.5
1	15	4.5
1	30	6.5

The best intercept at zero solidity is above the value of $\underline{K}$ for air, similar to their locations in Figures 1 and 2 for basalt. The intercepts at $\gamma = 1$ are not well determined.

The plot for air-saturated sandstones in Figure 8 shows isopleths of quartz content which are fairly close to the approximate ones given here in Figure 3, and so Figure 8 can be used for porous felsic igneous rocks. In addition, Figure 9 for water-saturated sandstones also can probably be used for porous, water-saturated, felsic igneous rocks without great error.

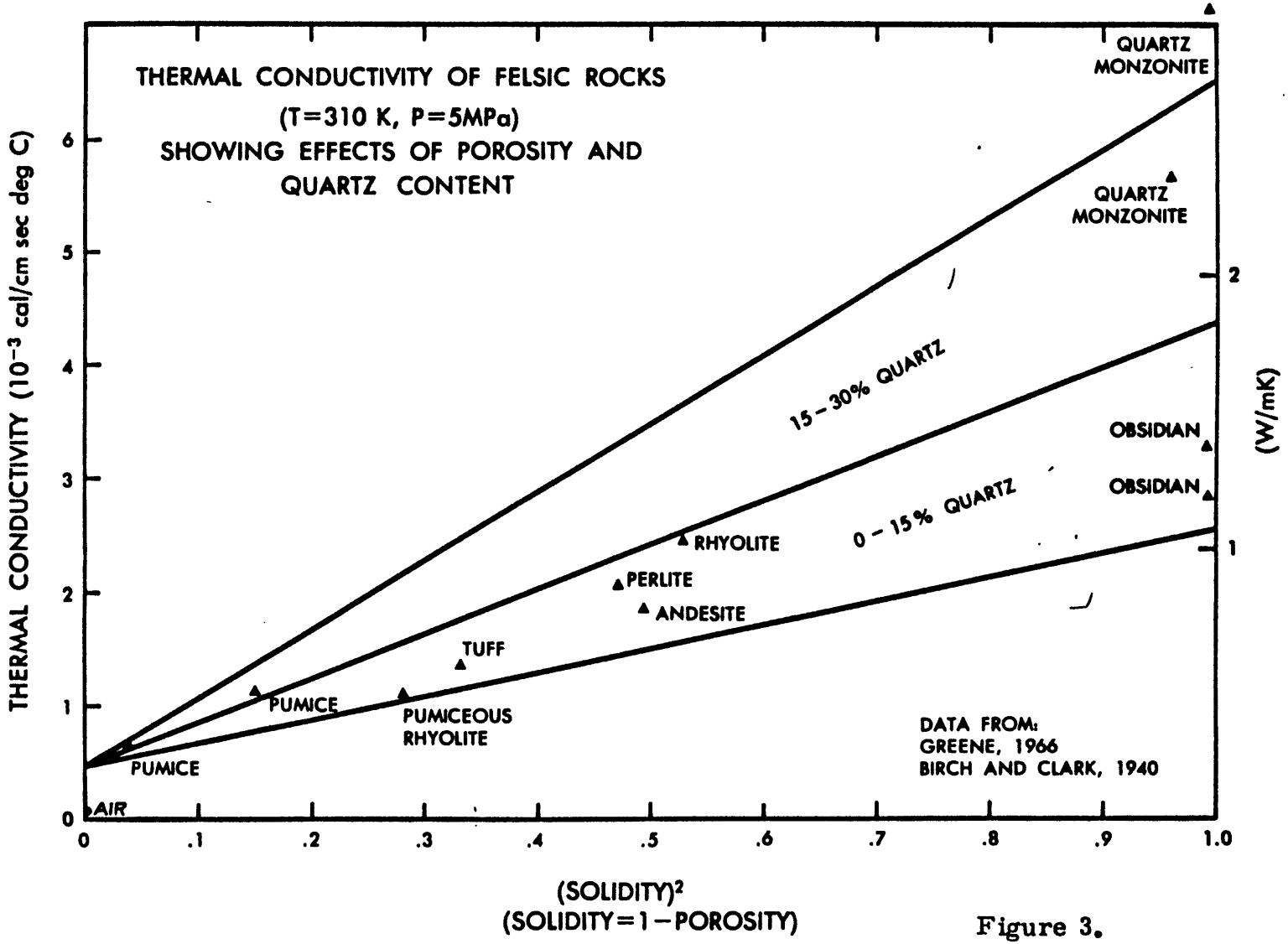

Figure 3.

(Robertson)

Figure 4.

The samples of limestone, on which measurements were made to provide the points plotted in this figure, were relatively pure calcite. The $\underline{K}$ intercept at $\underline{\gamma} = 0$ for air (.063 CU) seems acceptable; however, as with basalt, the $\underline{K}$ intercept at $\underline{\gamma} = 1$ is about 2 CU below the average for calcite crystal. The calcite samples were measured by Horai (1971) and by Birch and Clark (1940). The limestone measurements were made by Clark (1941), Zierfuss and Vliet (1956), Zierfuss (1969), and Beck et al (1971); the point at the highest $\underline{\gamma}^2$ is an average of 41 samples, measured by Robertson (1959).

The intercepts are as follows.

$\underline{\gamma}$	$\underline{K}$ (CU)
0	0.063
1	6.40

Figure 5.

Relatively pure calcitic limestone samples were used for the data used in preparing this figure, also. Although there is some scatter, the linear variation of $\underline{K}$ with $\underline{\gamma}^2$ seems fairly well established by the data. The intercept $\underline{K} = 1.48$ CU, the value for water, fits the trend reasonably well at $\underline{\gamma}^2 = 0$, and as with limestone in Figure 4, the intercept at $\underline{\gamma}^2 = 1$ is less than the single crystal measurements (Horai, 1971; Birch and Clark, 1941). The data plotted here are from Clark (1941), Bullard and Niblett (1951), Misener et al (1951), Zierfuss and Vliet (1956), and Beck et al (1971); the point at $\underline{\gamma}^2 = .99$, $\underline{K} = 6.75$ CU, is an average of 41 samples, measured by Robertson (1959).

The intercepts are

$\underline{\gamma}$	$\underline{K}$ (CU)
0	1.48
1	7.10

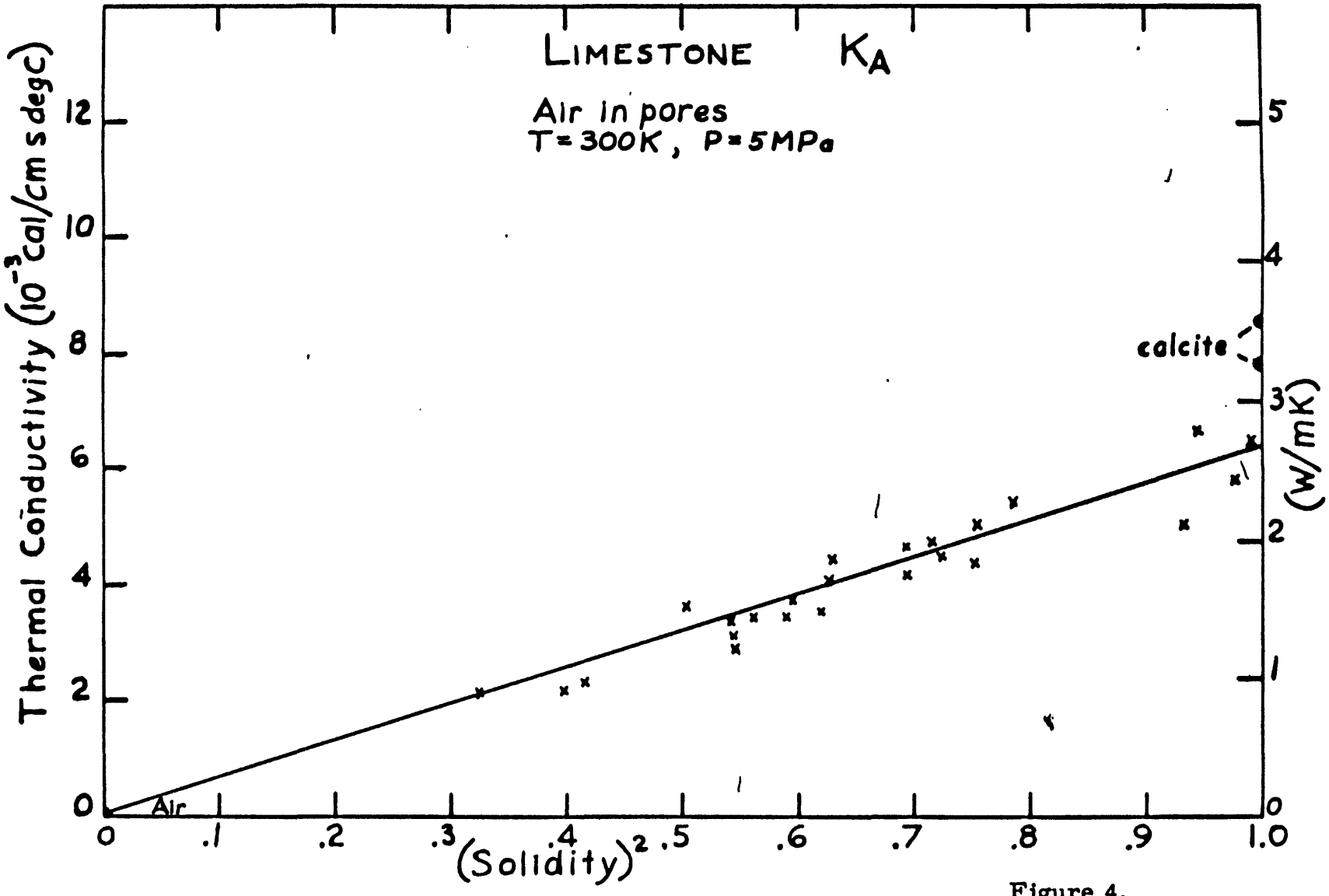

Figure 4.
(Robertson)

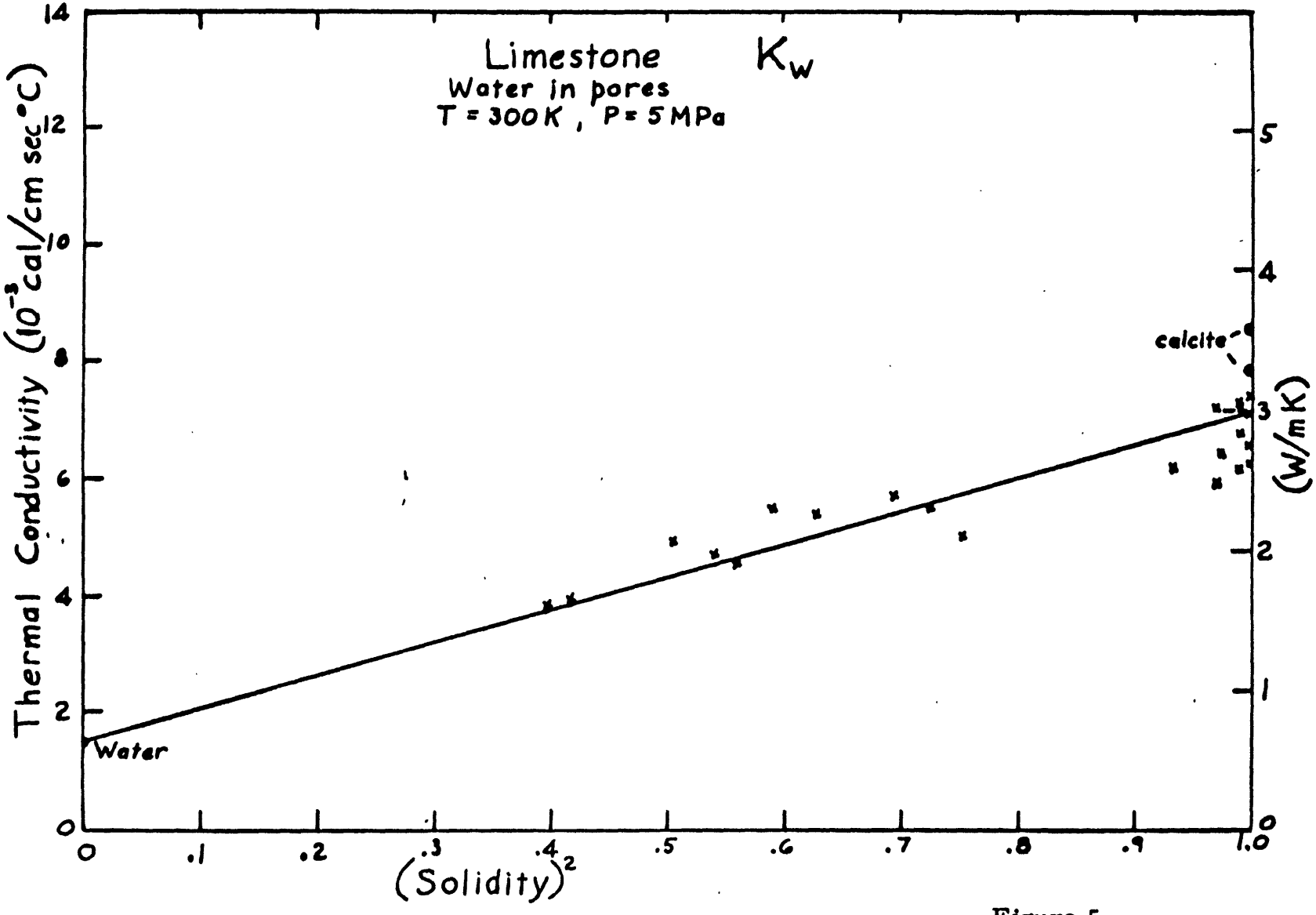

Figure 5.

(Robertson)

Figure 6.

The data for dolomite rock with air in the pores define a line through K for air (0.63 CU) at $\gamma^2 = 0$, and an intercept of K considerably less than the single crystal average. The dolomite crystal measurements were made by Horai (1971) and by W. H. Diment (written communication, 1968). The central data points are from Zierfuss (1969); the higher point, at $\gamma^2 = 0.90$, is from Bullard (1939), and the lower one at $\gamma^2 = 0.95$, is an average of 52 samples from Robertson (1959).

The intercepts are

γ	K (CU)
0	0.063
1	10.20

Figure 7.

Aside from the single crystal measurements on dolomite by Horai (1971) and Diment 1964 there is only one point on water-saturated dolostone. This value is an average of measurements made on 52 samples of fairly pure dolomite rock by Robertson (1959).

The intercepts are

γ	K (CU)
0	1.48
1	11.40

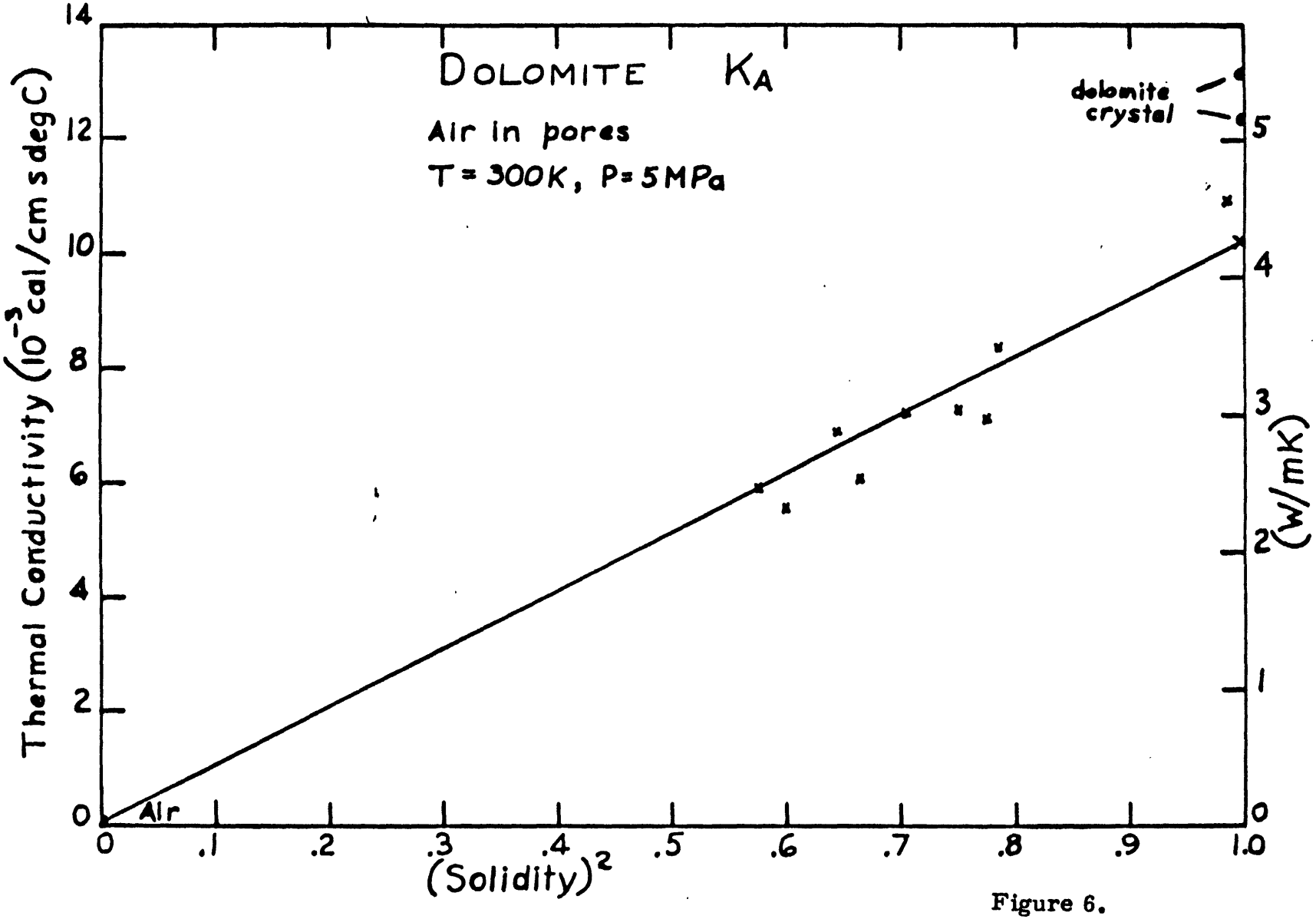

Figure 6.
(Robertson)

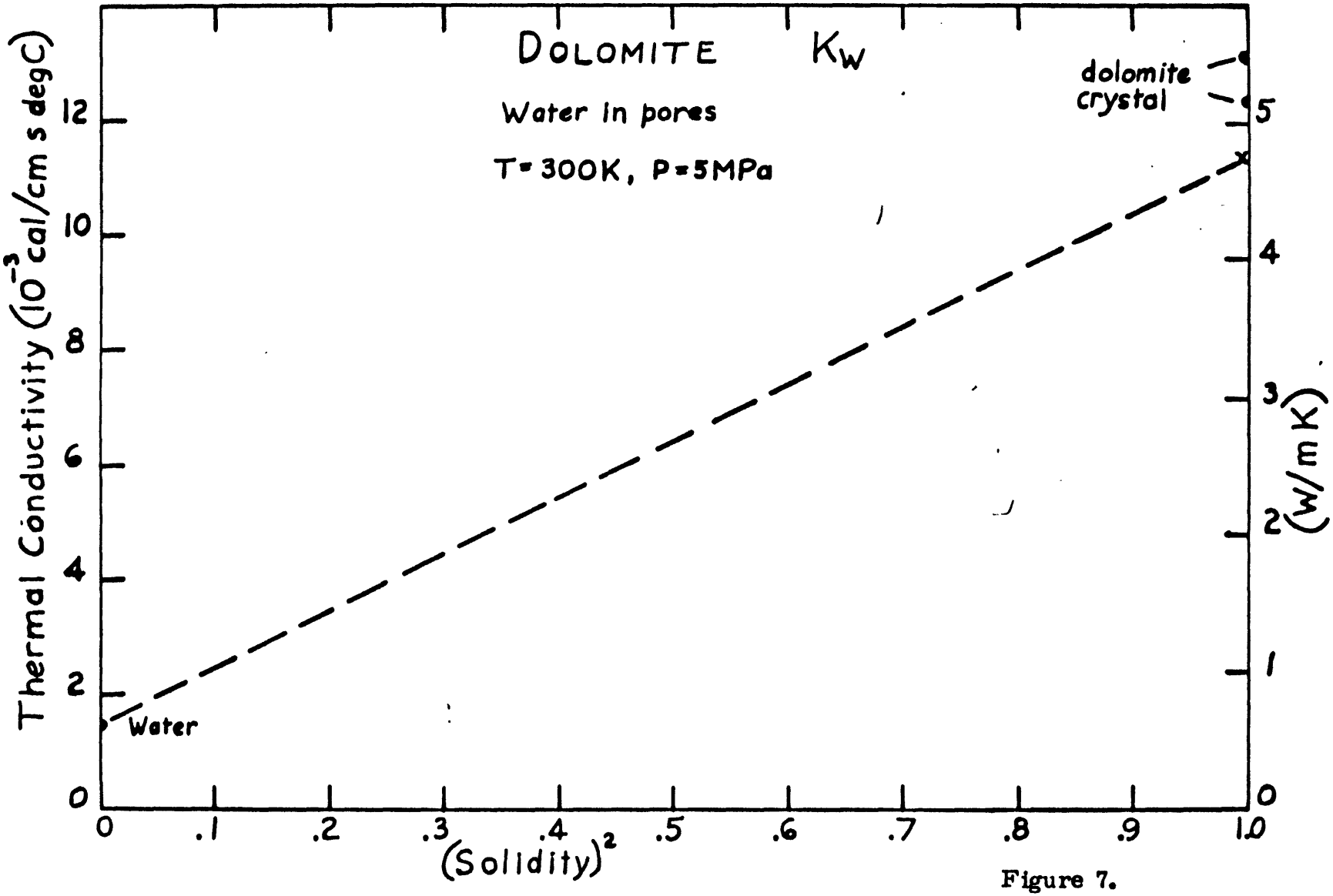

Figure 7.
(Robertson)

Figure 8.

The effect of raising $\underline{K}$ by increase of quartz content in sandstone is clear in Figure 8; the volume percentages of quartz are marked adjacent to the points. Unfortunately, only a few investigators did petrographic work on these air-saturated samples, but by adding to those data the requirement of internal-consistency of pairs of measurements made on the same samples with air (Fig. 8) and then with water (Fig. 9) in the pores, this graph could be prepared. As clay content is usually low, the lowering of $\underline{K}$ by clay is estimated to be small in these sandstones. As with basalt, the matrix of non-quartz minerals, mostly feldspars, are assumed to vary uniformly with solidity, so that only the quartz content need be known.

The measurements of single crystal quartz of Birch and Clark (1940) were used to calculate the average K = 17.90 CU for quartz shown in Figure 8 at $\gamma^2 = 1$. The range is from 14.62 CU to 24.36 CU, perpendicular and parallel to the C-axis respectively. The high values in Figure 8, above the 100 percent quartz line, are probably for well-cemented sandstones with preferred grain orientations of their C-axes in the heat flow direction.

The measurements of $\underline{K}$ on sandstones used in preparing this graph were made by Bullard (1939), Clark (1941), Zierfuss and Vliet (1956), P. E. Byerly (written communication 1958), Woodside and Messmer (1961) Sugawara and Yoshizawa (1961, 1962), Sucharev and Sterlanko (1970), and Anand et al (1973).

The locations of the isopleths are rather arbitrary, being forced to intercept the value for air, $\underline{K}$ = .063 CU, at $\gamma^2 = 0$, and being evenly spaced; with additional petrographic data on samples measured for $\underline{K}$, the locations could undoubtedly be improved. The intercepts are

	Quartz (Vol. %)	$\underline{K}$ (CU)
0	0	.063
1	0	3.50
1	100	12.50

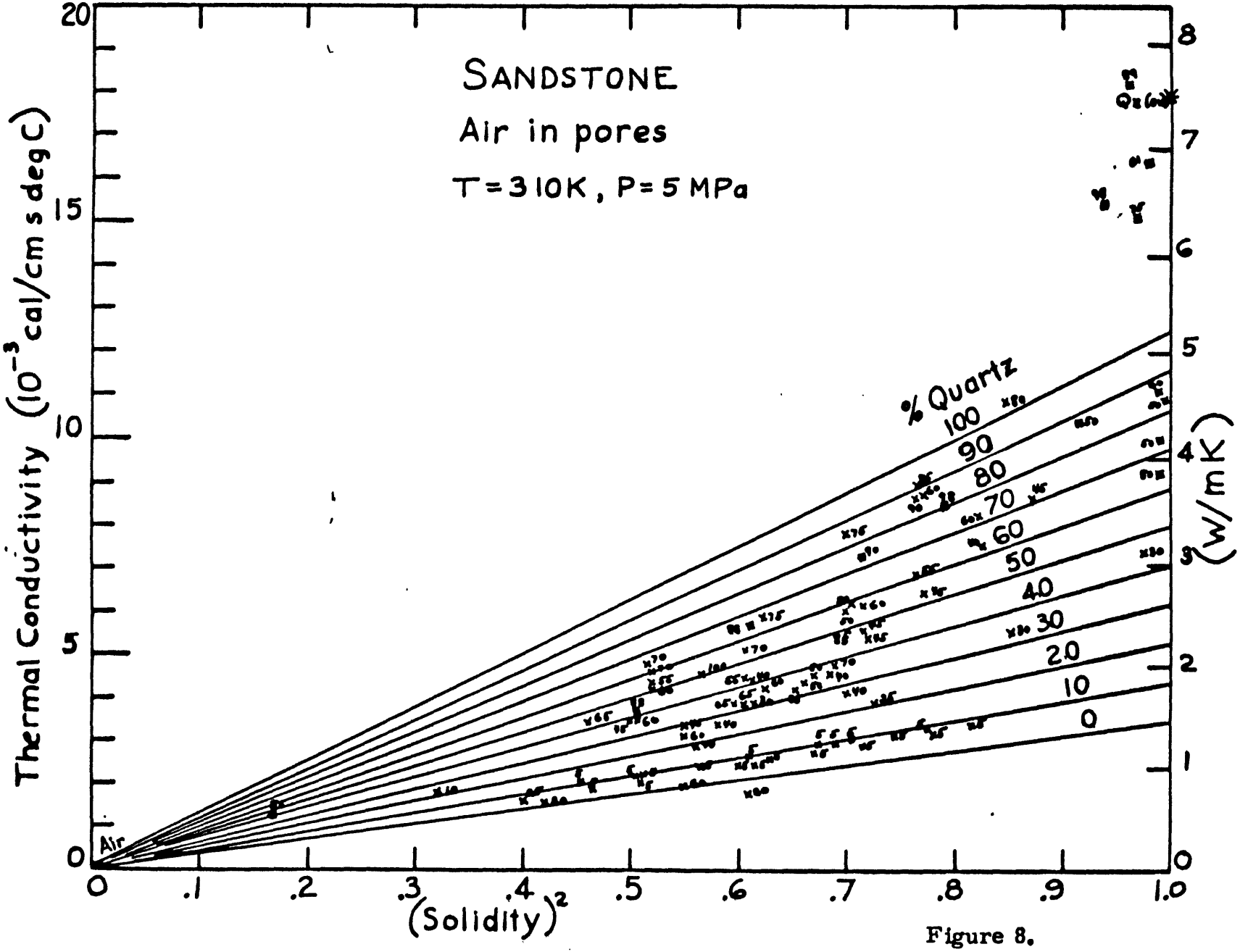

Figure 8.
(Robertson)

12a

Figure 9.

With water saturating the pores of sandstone, the effect shown here of raising the $\underline{K}$ with increasing quartz content is much enhanced over air-saturated pores (Fig. 8). Quartz percentages are placed adjacent to the points. The self-consistency in quartz contents of pairs of measurements in Figures 8 and 9 is useful, but there are many more sample modes available for this plot than for Figure 8. Clay content is usually low and so not important in lowering $\underline{K}$ of water-filled sandstones.

The average value for quartz crystal, $\underline{K}$ = 17.90 CU, falls near the 100 percent quartz intercept at $\gamma^2 = 1$, although such corroboration is not found in the other rock charts. The single crystal measurements were made by Birch and Clark (1941).

The data used to make this chart are from Clark (1941), Bullard and Niblett (1951), Asaad (1955), Zierfuss and Vliet (1956), Kunii and Smith (1961), Woodside and Messmer (1961), Sugawara and Yoshizawa (1961, 1962), Hutt and Berg (1968), and Anand et al (1973).

The intercepts are

γ	Quartz (Vol. %)	K (CU)
0	0	1.48
1	0	3.63
1	100	19.35

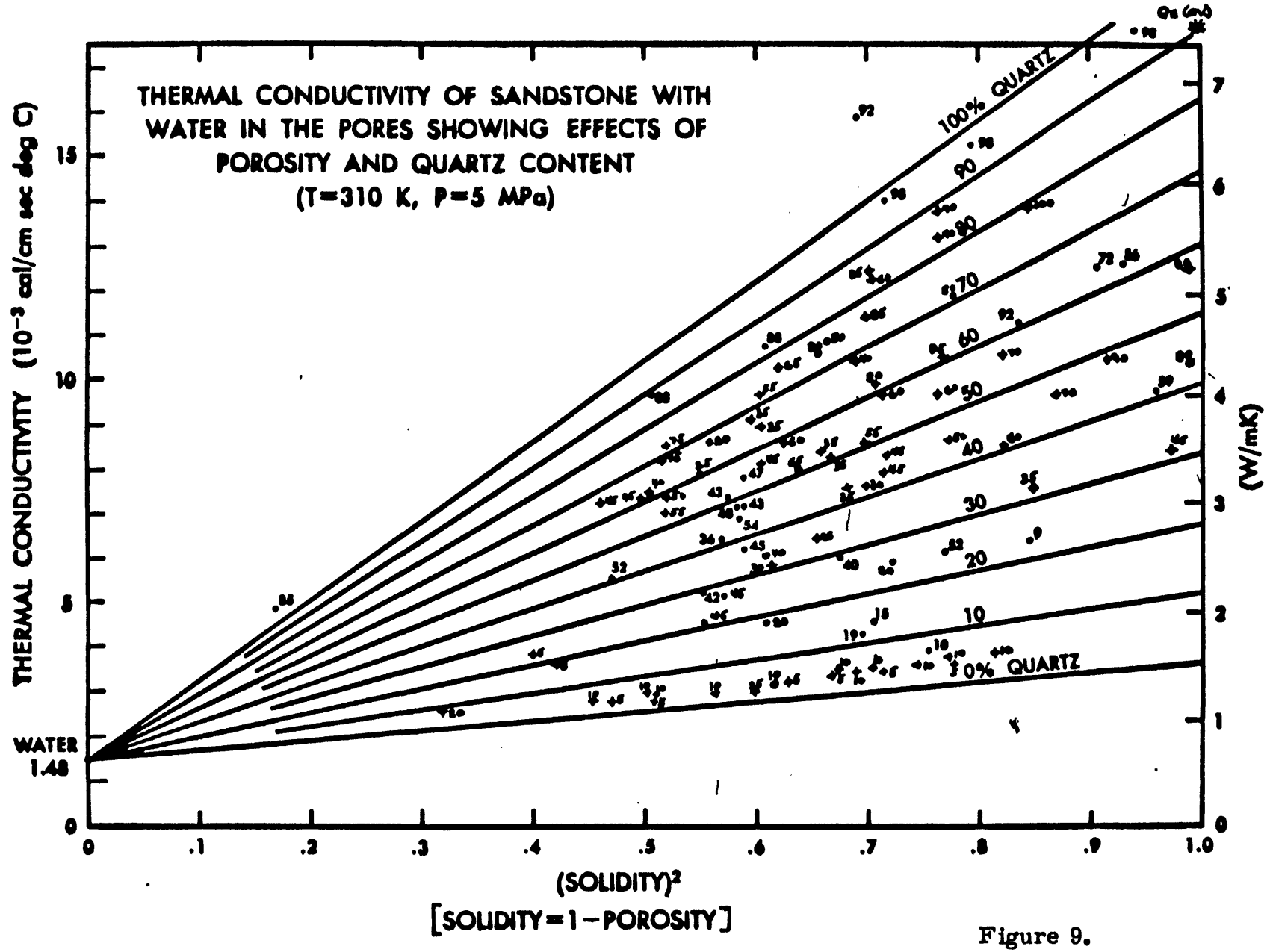

Figure 9.
(Robertson)

Figure 10.

In Figure 10 for water-saturated shale, and soil, the display of isopleths of quartz content is taken from the sandstone plot of Figure 9. By using the sandstone relations of $\underline{K}$ to quartz content, it is possible to estimate the effect of clay mineral content, of illite, montmorillonite, and kaolinite in decreasing the $\underline{K}$ of shale. The feldspar content in both sandstone and shale is assumed to be constant in affecting $\underline{K}$. The lowering of $\underline{K}$ is due to the low conductivity of clay and mica minerals perpendicular to the layering of the flakes, ($\underline{K}_{perp}$ = 1 CU, $\underline{K}_{para}$ = 8 CU), to the presence of many air-filled pores between flakes, and to the pore size being smaller than the mean free path of air molecules, thus preventing convection.

This graph is derived from measurements of shaley rock, comprised of the points of $0.5 < \underline{\gamma}^2 < 1$, and of shaley soil, for which $0.12 < \underline{\gamma}^2 < 0.5$. The "X" points for the soils and shales are marked with quartz content above and clay content below. The triangle points at $0 < \underline{\gamma}^2 < 0.17$ are for oceanic muds from ~~Radcliff~~ Ratcliffe (1960, and in Clark, 1966) and Butler (in Clark, 1966); no petrographic data are available on them.

The soils data are from Kersten (1949), Higashi (1952), and Penner (1963). A number of samples were measured by Penner (1963) both vertically across the bedding (and clay flake layering) and horizontally, parallel to it; the points are marked "v" and "h" respectively, at the same $\underline{\gamma}^2$ value, separated by a difference of about $\Delta \underline{K} = 0.5$ CU; this shows the anisotropy in $\underline{K}$ in these soils, due to the clay primarily.

The shale points (Fig. 10) marked by a star between quartz content lines of 0 and 10 percent, are from Benfield (1947). The quartz values above the points of Benfield are the isopleth values from Figure 11 for the same shale samples saturated with air; this internal-consistency method of finding quartz values was used for certain sandstone points also (Figs. 8 and 9). The dot points lined up at about $\underline{\gamma}^2 = 0.72$ are from a suite of shales measured by King and Simmons (1972); no modes are given. The nearly vertical line at $\underline{\gamma}^2 = 0.97$ is from Sucharev et al (1972) and shows the spread of values for 6 samples of aleurite, containing 55 to 70 percent quartz. Other data on shales are from Bullard and Niblett (1951), Beck and Beck (1958), and Zierfuss (1969). The square point at

$\underline{\gamma}^2$ = 0.72, $\underline{K}$ = 2.41 CU, is from J. Combs and C. Swanberg (written communication, 1975); it is their "best clay" calibration value for shales, and is for a layer containing 95 percent clay minerals.

The following generalized scheme can be used to account for the quartz and clay effects on $\underline{K}$ for shales or soils with known solidity. The method involves correcting the quartz content for the clay content to a fictive value for quartz and then using the sandstone isopleths of quartz to find the value of $\underline{K}$ at the given $\underline{\gamma}^2$. The effect of anisotropy is neglected; only values of $\underline{K}$ normal to bedding are considered. For soil broken up from its natural state and reconstituted, there seems to be only a slight reduction in $\underline{K}$ by the clay minerals, and thus no anisotropy.

For shales and soils with quartz content more than 35 percent, the clay content is usually less than 30 percent, and for such shales the modal content of quartz would be reduced one-for-one by the modal clay content to attain a fictive value of quartz to use on the graph, (Fig. 10). For example, with qz = 50 °/₀ , clay = 15 ° /₀ , the fictive qz = 35 °/₀ , the number to use on Fig. 10 to obtain the $\underline{K}$.

For shales and soils with quartz content less than 35 percent, the clay may range from low to high in proportion, but the clay apparently is not so effective in reducing $\underline{K}$. The following scheme may be used (albeit with great uncertainty). Subtract 20 percent from the clay content, and then subtract any remainder percentage of clay from the quartz percentage to obtain the fictive value of quartz to use on the graph (Fig. 10). For example, with qz = 30 °/₀ , clay = 60 °/₀ , the fictive value of quartz would be qz = 30 - (60-20) = -10 °/₀ , and thus the value of K would be below the zero quartz isopleth by 10 percent at the given $\underline{\gamma}^2$. This scheme badly needs supportive or amending data.

The intercepts for the quartz content isopleths are the same as for water-saturated sandstone (Fig. 9).

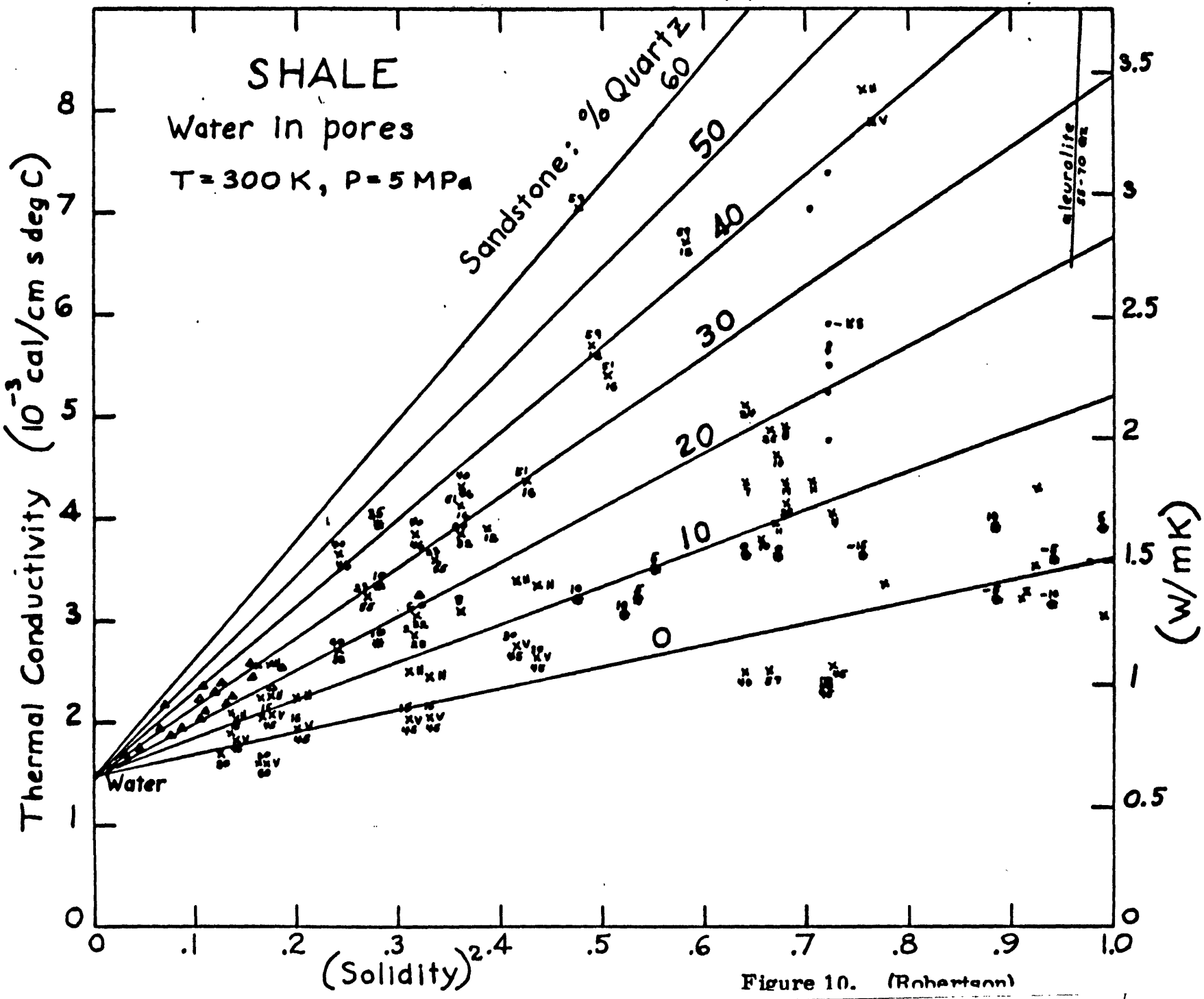

Figure 10. (Robertson)

Figure 11.

As in Figure 10, the quartz isopleths in this shale plot are the same as those of the air-saturated (i.e. dry) plot of sandstones in Figure 8. There is no petrographic information at hand for the samples measured; the values of $\underline{K}$ for points between 5 to 10 percent quartz are from Figure 10 (Benfield, 1947) and are the internal-consistency values. The other, unmarked observations for shale samples with air in the pores are from Bullard (1939), Benfield (1947), and Mossop and Gafner (1951). The points marked "h" and "v" are measurements, parallel and perpendicular (horizontal and vertical) to bedding, made by Beck and Beck (1958), which show that the anisotropy of their sample is much greater with air in the pores than with water there (see Fig. 10).

Without observations of quartz and clay content, the data plotted in Figure 11 for dry shale cannot be analyzed for the effect of quartz and clay on $\underline{K}$. The values at the data points from Benfield (1947) in Figure 10 and 11 are only relative and are not absolute quartz percentages; the unknown amount of clay in the shales would certainly decrease $\underline{K}$ below the amount that would be predicted using only the actual quartz content and the sandstone isopleths in Figure 11. Similarly, the other points plotted are positioned at $\underline{K}$ values determined by the amount of clay as well as quartz in each sample.

Lacking a clear relationship for air-saturated shale, the scheme evolved for water-saturated shale to account for the effect of clay and to find a fictive quartz value may be used (see Fig. 10). Intercepts of the isopleths in Figure 11 are the same as those for air-saturated sandstone in Figure 8.

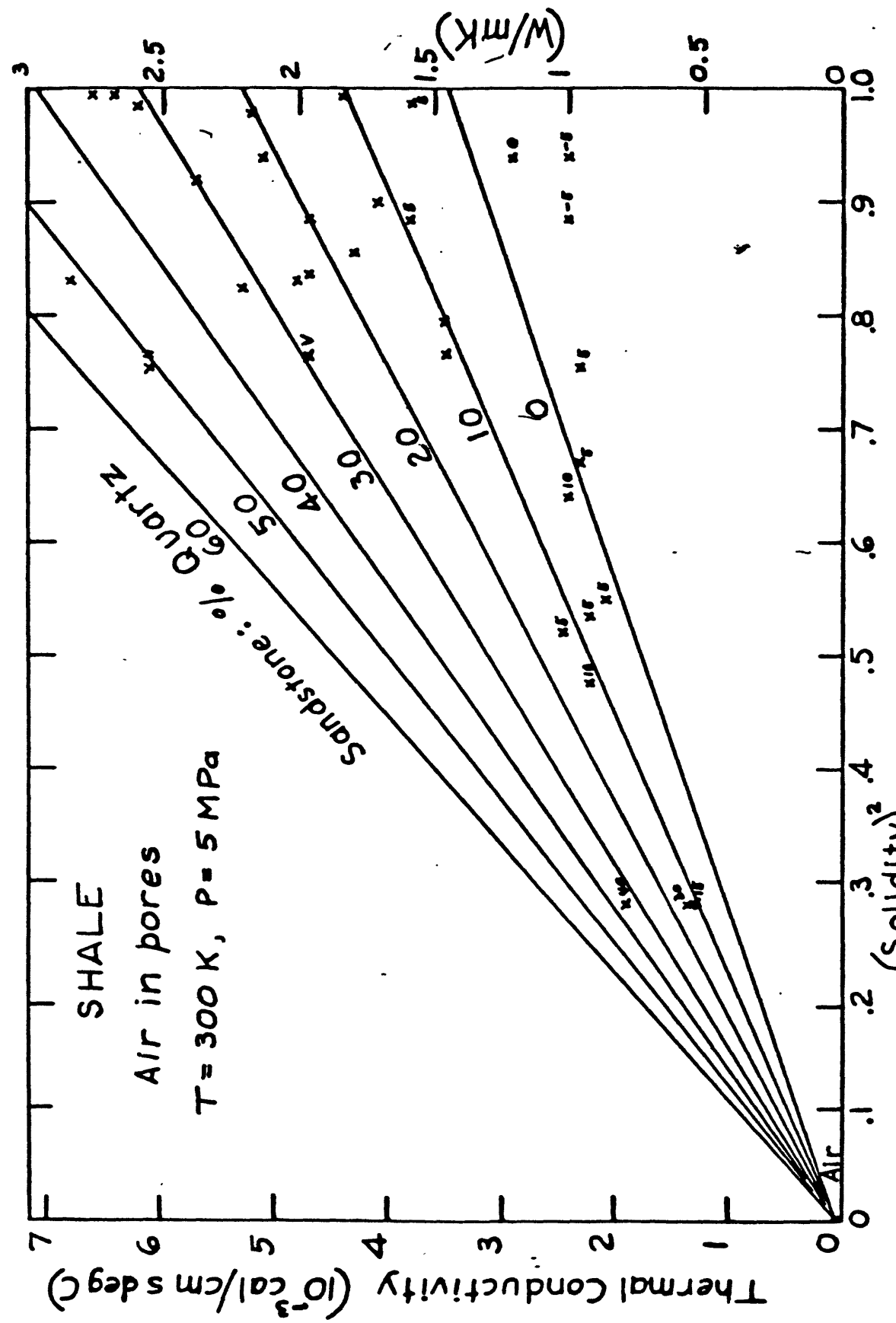

Figure 11.
(Robertson)

Figure 12.

The values of $\underline{K}$ for dry soils, most of which can be considered as unconsolidated shales, are very much lower than those for dry shales. In Figure 12 a tentative set of isopleths has been drawn (full lines) to fit the quartz content only of the dry soils, as was done with the sandstone data in Figure 8; the lower three isopleths from Figure 8 are shown as dashed lines. Similarly also, fictive quartz values can be obtained to estimate $\underline{K}$ in Figure 12 by subtracting the clay percentage (below the points) from the quartz percentage (marked in above the points). Thus for qz = 40 °/₀ and clay = 15 °/₀, the fictive qz = 25 °/₀, at the given $\underline{\gamma}^2$.

Data used in plotting are from Smith and Byers (1938), Kersten (1949), and Higashi (1952). The quartz and clay contents for points from Smith and Byers were calculated for a fixed mineral norm from chemical analyses of the soils.

The isopleths are forced through the $\underline{K}$ for air, and the pertinent intercepts are

$\underline{\gamma}^2$	Quartz (Vol. °/₀)	K (CU)
0	0	.063
1	0	0.84
1	100	2.49

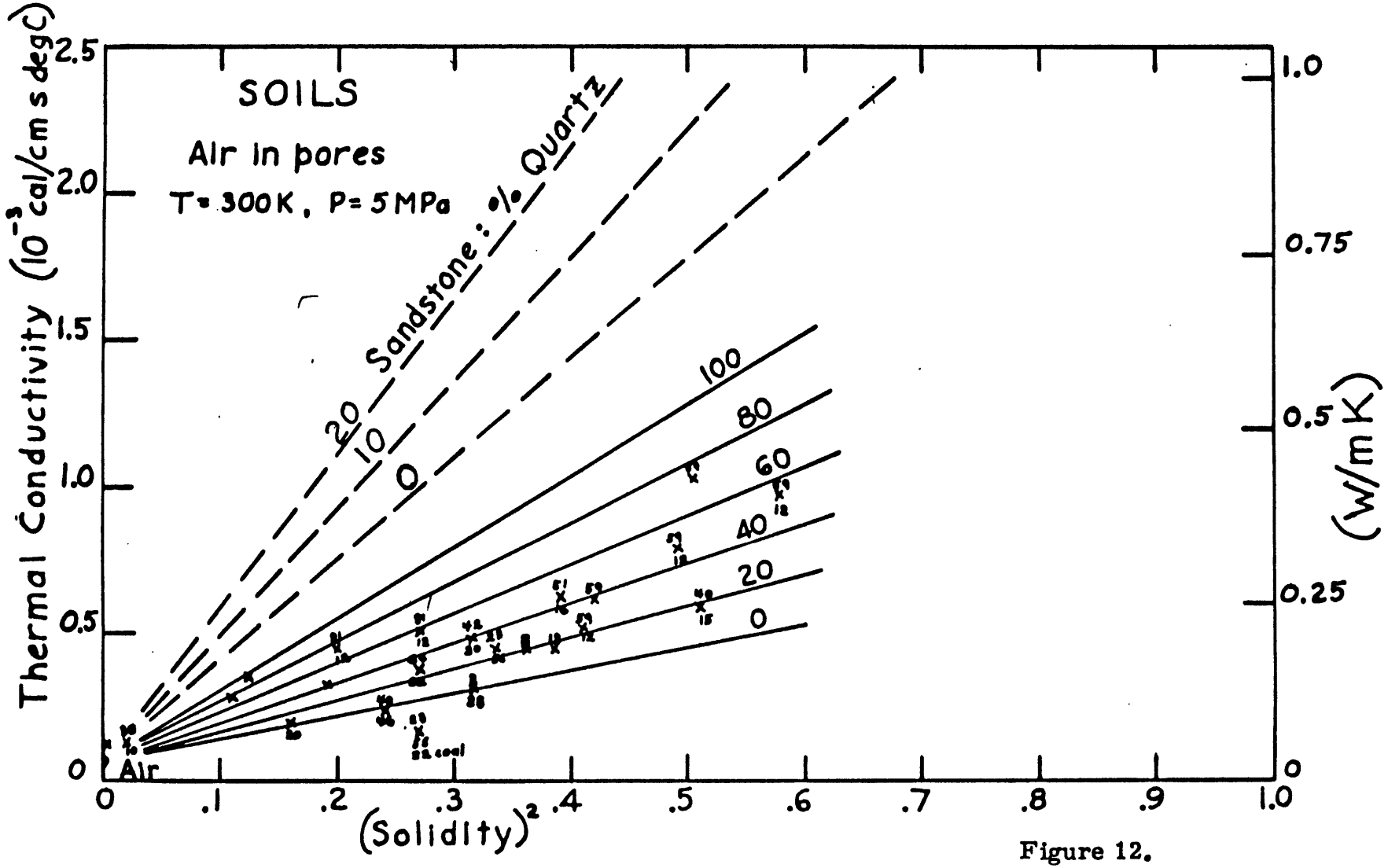

Figure 12.
(Robertson)

Figure 13.

This figure was prepared to aid in assessing the possible use of anhydrite beds as repository sites for radioactive waste, suggested by D. W. Stewart (oral communication, 1977). The points plotted in Figure 13 for $\underline{K}$ vs $\underline{\gamma}^2$ are for monomineralic aggregate samples of anhydrite and gypsum. The point for gypsum is from Horai (1971), and the points for anhydrite are from Eucken (1911), Coster (1947), Bullard and Niblett (1951), and Herrin and Clark (1956). Many measurements were made by Zierfuss (1969) on impure anhydrite rock samples, but the values are much lower, averaging about $\underline{K}$ = 8 CU at $\underline{\gamma}$ = 0.95, and are not plotted; the rock probably contains considerable gypsum.

The lines of variation with $\underline{\gamma}^2$ are forced through the value for air, and the intercepts are

	$\underline{\gamma}^2$	$\underline{K}$ (CU)
gypsum	0	.063
	1	3.15
anhydrite	0	.063
	1	14.12

The inset drawing shows the effect of temperature on $\underline{K}$ of anhydrite and of some reference minerals and rocks, quartz, halite, granite, and basalt. The purpose of adding this inset is also to aid in radioactive waste assessments. The measurements on anhydrite were made by Weber (1895) from 0° to 110° C, with a slope of -2.95 CU/100° C. The other curves are taken from Figure 14 for basalt, Figure 15 for the granite, Figure 20 for quartz, and Figure 21 for halite; the basalt has 11 percent porosity, but the other materials are quite dense.

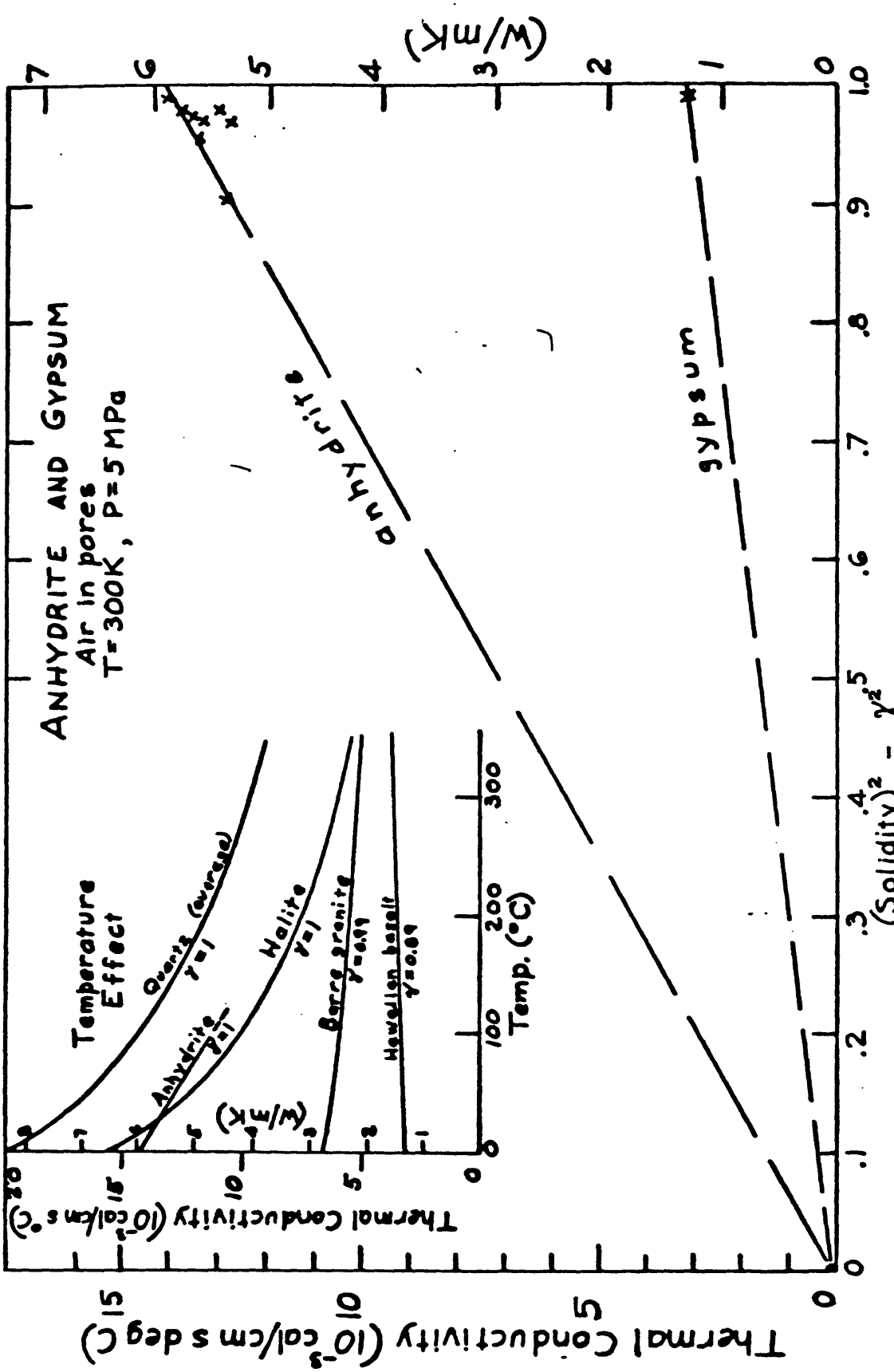

Figure 13.
(Robertson)

The Temperature Effects on Thermal Conductivity

The thermal conductivity K of most rocks decreases with increase in temperature T, ranging from slight to -30 percent in the first 100° C. Basalt increases slightly with temperature.

In the following explanations of figures, the measurements and their sources are described. In general, these plots of T vs K for the principal rock types can be used by ascertaining first the K at some T, by actual measurement or by estimation from the previous charts (T = 30° C) (Figs. 1 - 13). Then, using these K vs T plots, follow the curve passing nearest the estimated K value to the T of interest.

The data in these figures are from laboratory observations, so heat transfer by all mechanisms is included, by solid conduction, radiation, and convection of fluids in the pores.

Figure 14.

The upper curves in this figure are from Birch and Clark (1940) from data on intrusive, dense diabase samples, whereas the other curves and points are from extrusive basalts. The other references for the data given on Figure 14 include Poole (1914), Bridgman (1924), Stephens (1963), Kawada (1966), Kanamori et al (1969), Petrunin et al (1971), Robertson and Peck (1974), and Peck et al (1977). The numbers in parentheses on Figure 14 are decimal porosities.

The slope of the line from Peck et al (1977), 0.19 CU/100° C, may be taken as an average for vesicular basalt. It is subparallel with Kawada's line, and falls on the trend of Stephen's points (triangles). In general, the effect of temperature on the K of basalt, including diabase and dolerite, can probably be ignored for approximate estimates to about 500° C.

Figure 15.

The curves in this drawing are derived from the data on selected, felsic igneous rocks, named on appropriate curves, measured by Birch and Clark (1940). Although they suggested using thermal resistivity (reciprocal of K) for extrapolation and interpolation, the conductivities are

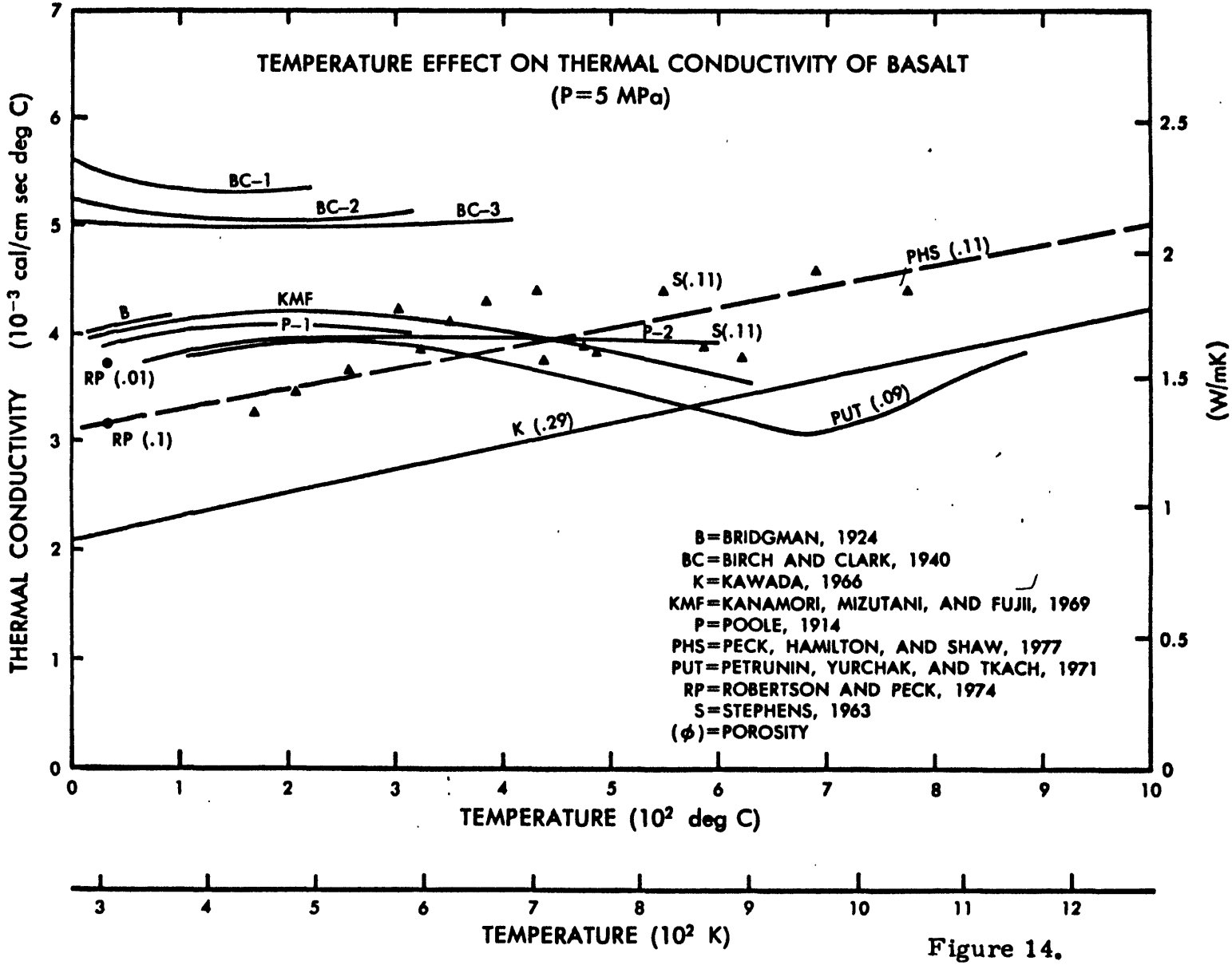

Figure 14.
(Robertson)

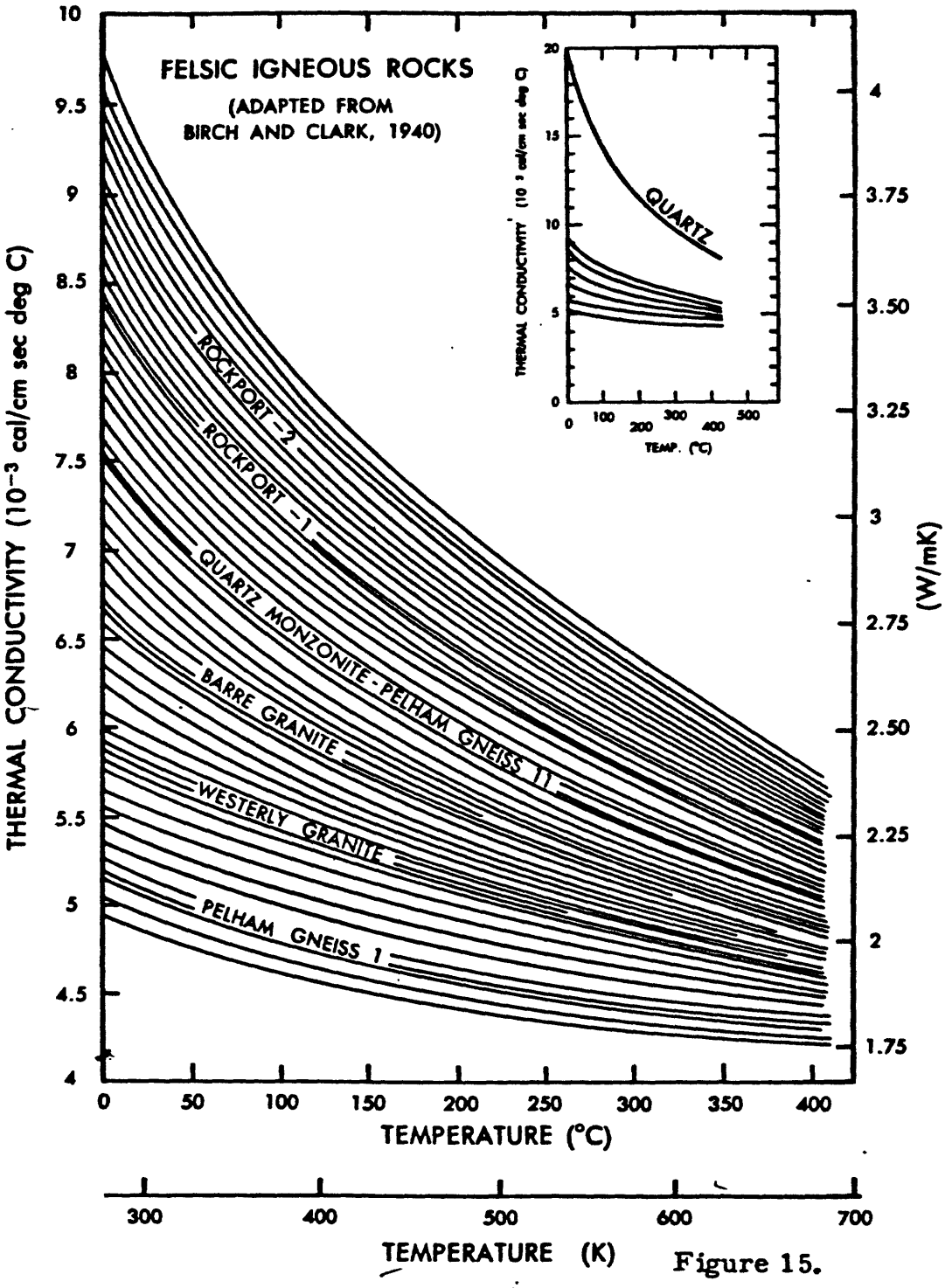

Figure 15.
(Robertson)

plotted in Figure 15 to emphasize the family character of the curves, including average quartz, as shown by the inset figure, and for ease of getting $\underline{K}$ values. The curves' locations are determined grossly by the quartz content; the anisotropy effect is shown by the two Pelham gneiss curves, parallel and perpendicular to the foliation of the mica minerals; the Rockport-2 granite is denser (with a density equal to the theoretical value) than Rockport-1. Birch and Clark (1940) discuss ways of calculating $\underline{K}$ from the modes of these rocks.

The interpolated curves were drawn to pass through values of $\underline{K}$ at 0.1 CU spacing at 35° C. With an estimated $\underline{K}$ at a given $\underline{T}$, the nearest curve to that point can be followed to estimate the $\underline{K}$ at some other $\underline{T}$.

Figure 16.

The temperature effect on the $\underline{K}$ of limestone and dolostone is negative, as shown in this figure. The curves marked "BC" are from Birch and Clark (1940); the letters following, "l", "m", and "d" mean limestone, marble, and dolostone; the symbols "$\parallel$" and "$\perp$" mean parallel and perpendicular to bedding; the number in parentheses represents solidity γ. The curves marked "M" are from Mirkovitch (1968); the letters "l" and "d" and the numbers in parentheses have the same meaning.

For single crystals at 30° C and 50 bars, average calcite $\underline{K}$ = 8.58 CU, and dolomite $\underline{K}$ = 13.16 CU (Horai, 1971). The rocks, limestone and dolostone, are seen to be lower in $\underline{K}$ than the mineral crystals (also described for Figs. 4 - 7); the effect of solidity in reducing $\underline{K}$ is also clear. The anisotropy due to bedding can have a fairly large effect on $\underline{K}$ of carbonate rocks (Fig. 16).

No effort has been made to draw interpolated curves on Figure 16. Estimates of the $\underline{T}$ effect on $\underline{K}$ can be made only roughly anyhow from this plot.

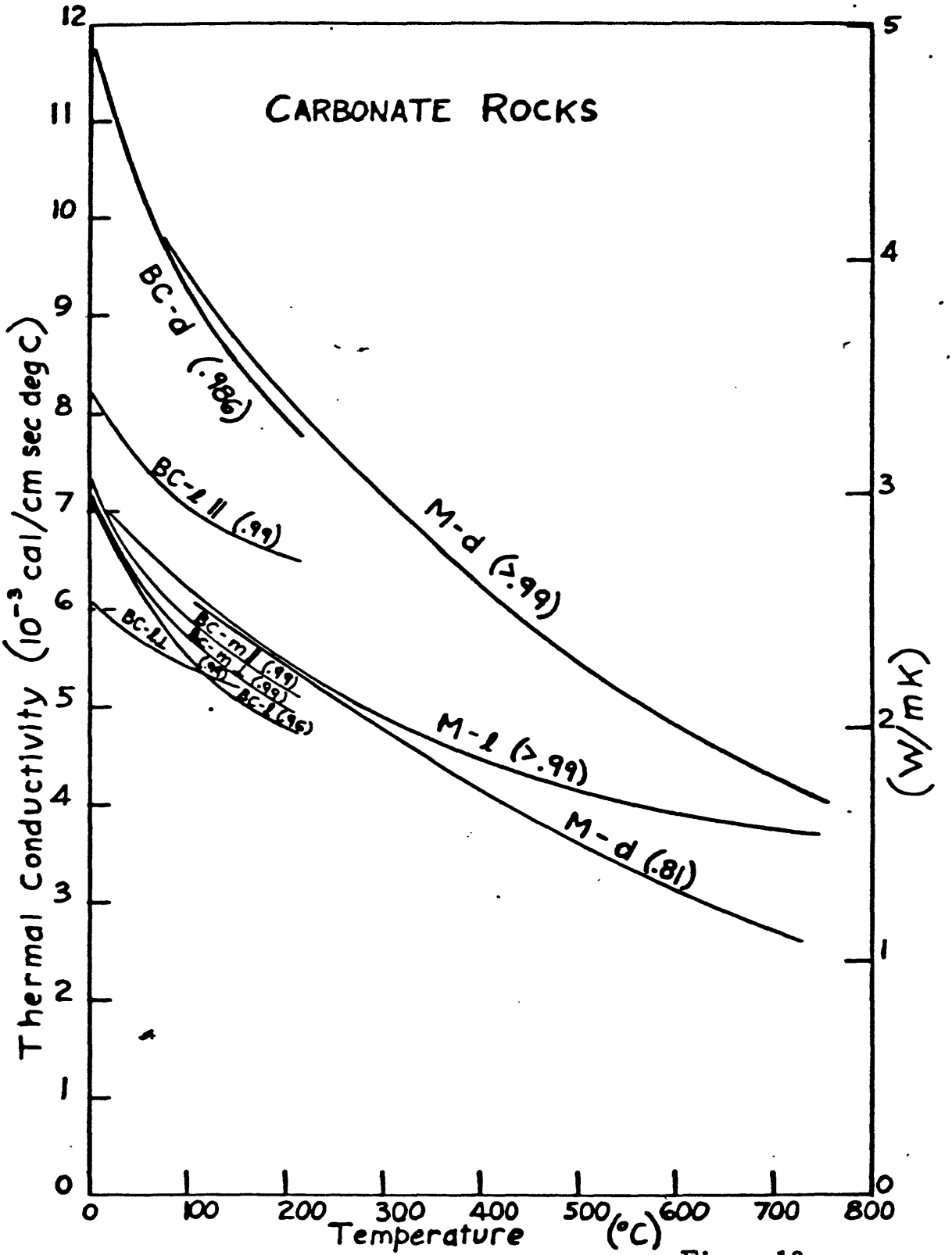

Figure 16.
(Robertson)

Figure 17.

The upper curves are for dense quartzites and single crystal quartz, and they show a marked negative temperature effect on $\underline{K}$. The curves marked "BC - qz" are from single crystal measurements, parallel (//) and perpendicular ($\perp$) to the C-axis, from Birch and Clark (1940); the average curve is obtained by weighting the data for "qz$\perp$" by a factor of 2. The anisotropy of the rather dense quartzite measured by Birch and Clark is not large (see curves marked "qt//" and "qt$\perp$"). The data for the curves marked "M - t" and "M - qt" are from Mirkovitch (1968) for dense taconite and quartzite.

The symbols on the curves at lower $\underline{K}$ for $\underline{T} < 200°$ C represent references, rock types, pore fluid type, and solidities, as follows. The letters "A", "BC", and "SY" are for Anand et al (1973), Birch and Clark (1940), and Sugawara and Yoshizawa (1961, 1962). The rock symbols are "ss" for sandstone, "sh" for shale, "sl" for slate; all "SY" curves are for sandstone. The pore fluids symbols are "a" for air and "w" for water. The decimal values of γ are given in parentheses. At values of $\underline{K} < 5$ CU, the temperature effect is low and either slightly positive or negative, depending on the rock type and the method of measurement. The same value for γ signifies that the same rock specimen was used for both air-and water-saturated measurements. Extrapolation of these low-temperature curves would be uncertain, although the $\underline{T}$ effect seems to be small for these porous rocks.

Figure 18.

The ultramafic rocks shown in this figure have negative temperature coefficients of $\underline{K}$. The curves are from the data of Birch and Clark (1940), marked "BC", and Kawada (1964, 1966), marked "K". The rock symbols are "hz" for harzburgite, "du" for dunite, "hy", for hypersthenite, "br" for bronzitite, "sp" for serpentinized peridotite, "p" for peridotite, and "ec" for eclogite. The numbers refer to different specimens taken from the same large sample.

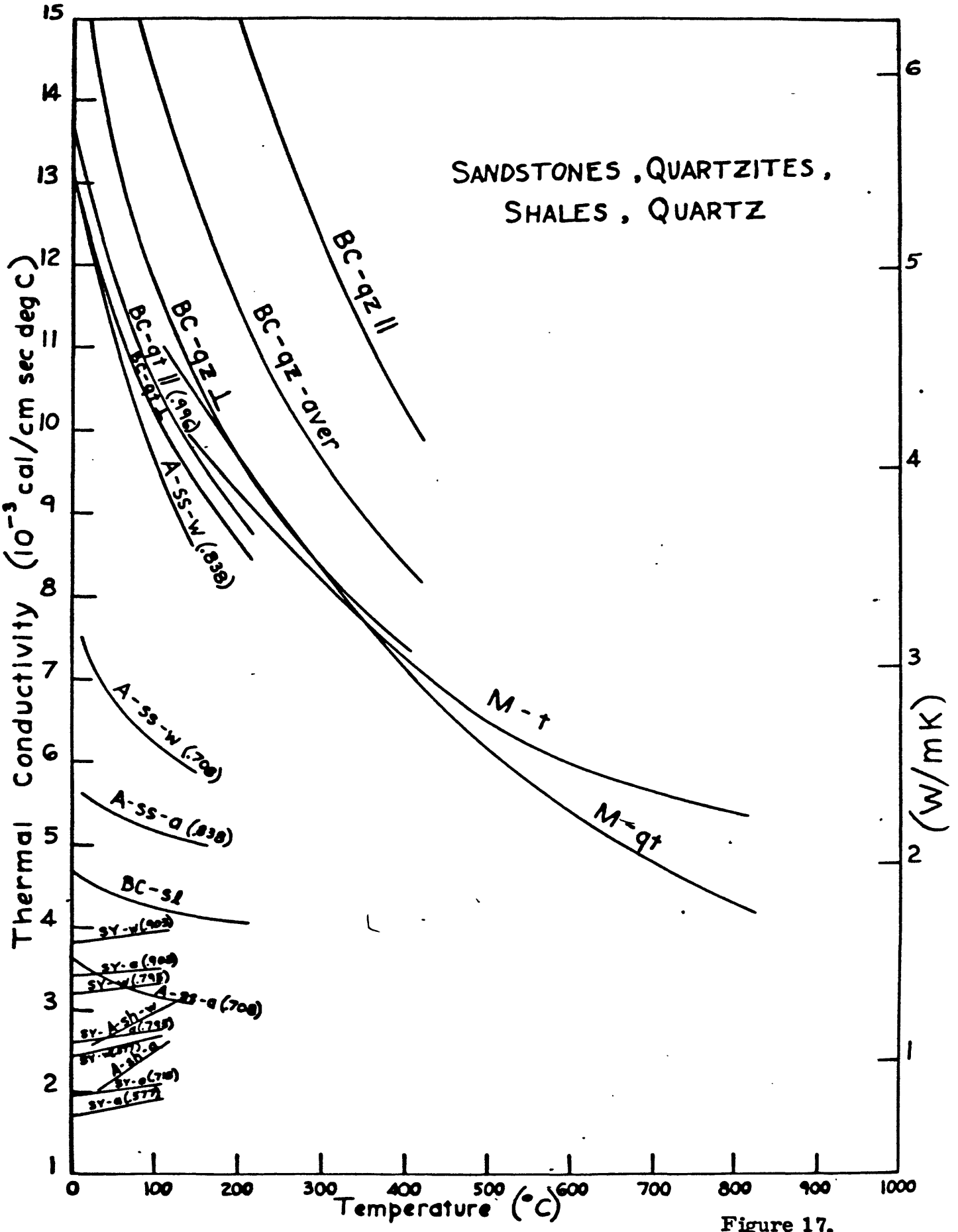

Figure 17.
(Robertson)

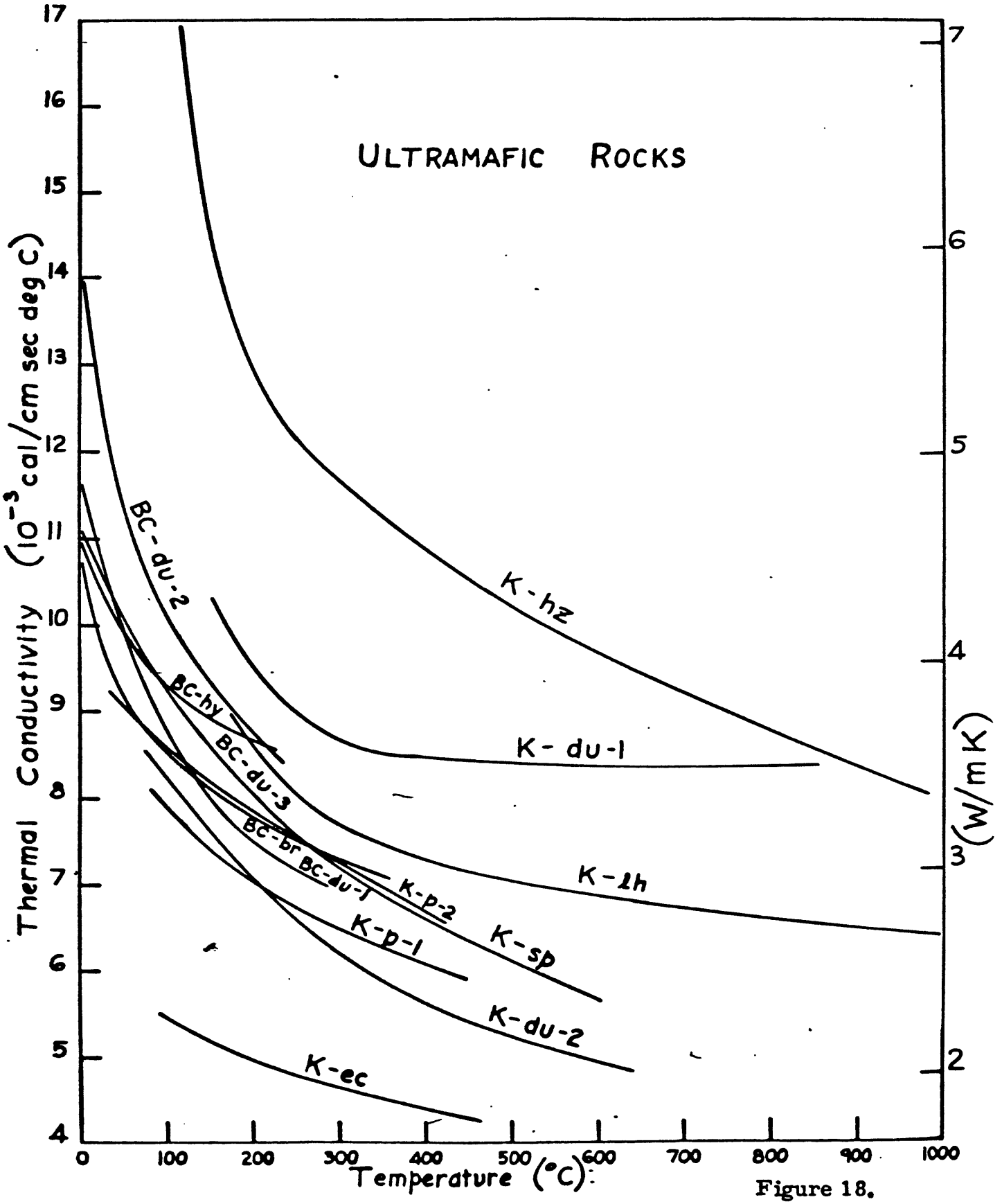

Figure 18.

(Robertson)

The absolute values of $\underline{K}$ of Kawada's harzburgite and dunite -1 curves in Figure 18 may be somewhat uncertain, as they extrapolate higher than the monomineralic aggregate value for forsterite at 30° C, $\underline{K}$ = 12.32 CU (Horai, 1971). A number of effects are not accounted for, such as, anisotropy of olivine grains due to preferred grain orientations, phenocryst versus fine grain differences, and conduction across fractures, pore, and grain-to-grain.

There is enough variety of rock type in Figure 18 that the curves may be used to estimate $\underline{K}$ roughly at some $\underline{T}$ for most, dense ultramafic rocks, starting with a known $\underline{K}$ and $\underline{T}$. To obtain a value of $\underline{K}$ for a porous ultramafic rock, a line of $\underline{K}$ vs γ^2, like that for limestone in Figure 4 or 5, can be constructed between a value taken from Figure 18 and $\underline{K}$ for air or water, and an interpolation mode.

There are a number of measurements on serpentine rock available from Diment (1964), but they are ambiguous, and they are not shown in Figure 18. The serpentinites have values around $\underline{K}$ = CU at 30° C, for 0.94 > γ > 1, and they have varying contents of brucite, magnetite, pyroxene, and olivine, as well as of the serpentine minerals.

Figure 19.

These curves are from Birch and Clark (1940). The positive temperature coefficient of $\underline{K}$ for commerical glasses is well-established, and so the slopes shown in Figure 19 are not surprising. (The anomalous temperature and pressure coefficients of the elastic moduli are well-known.) The values of $\underline{K}$ for the rock glasses shown and for most commercial glasses are about the same for $\underline{T}$ < 500° C, and so glasses for other rock compositions may be expected to have $\underline{K}$ values near the curves in this figure.

Figure 20.

Quartz occurs as phenocrysts in felsic igneous and metamorphic rocks and as large grains in sedimentary rocks, and the combinations of prevalence, large grain size, and high thermal conductivity of quartz make it the most important mineral to evaluate in estimating the thermal conductivities of rocks containing it. As described for Figures 3 and 8-12,

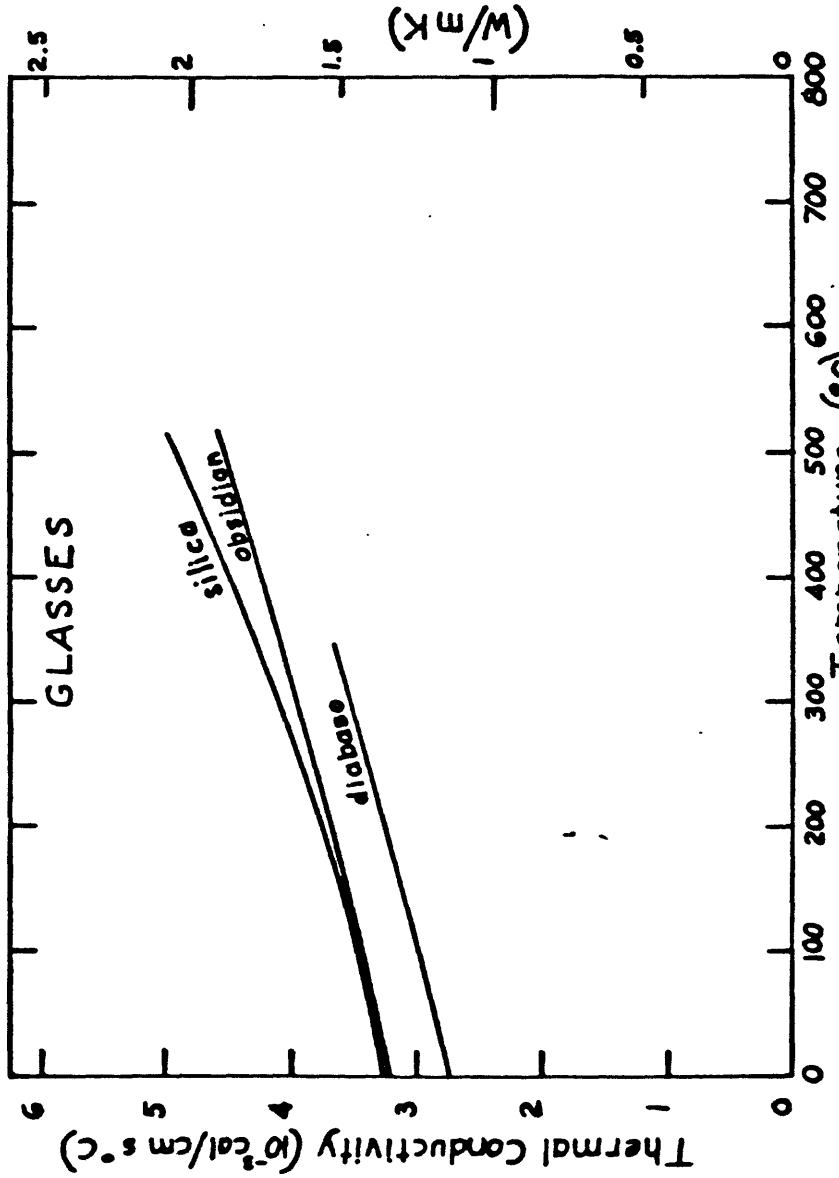

Figure 19.
(Robertson)

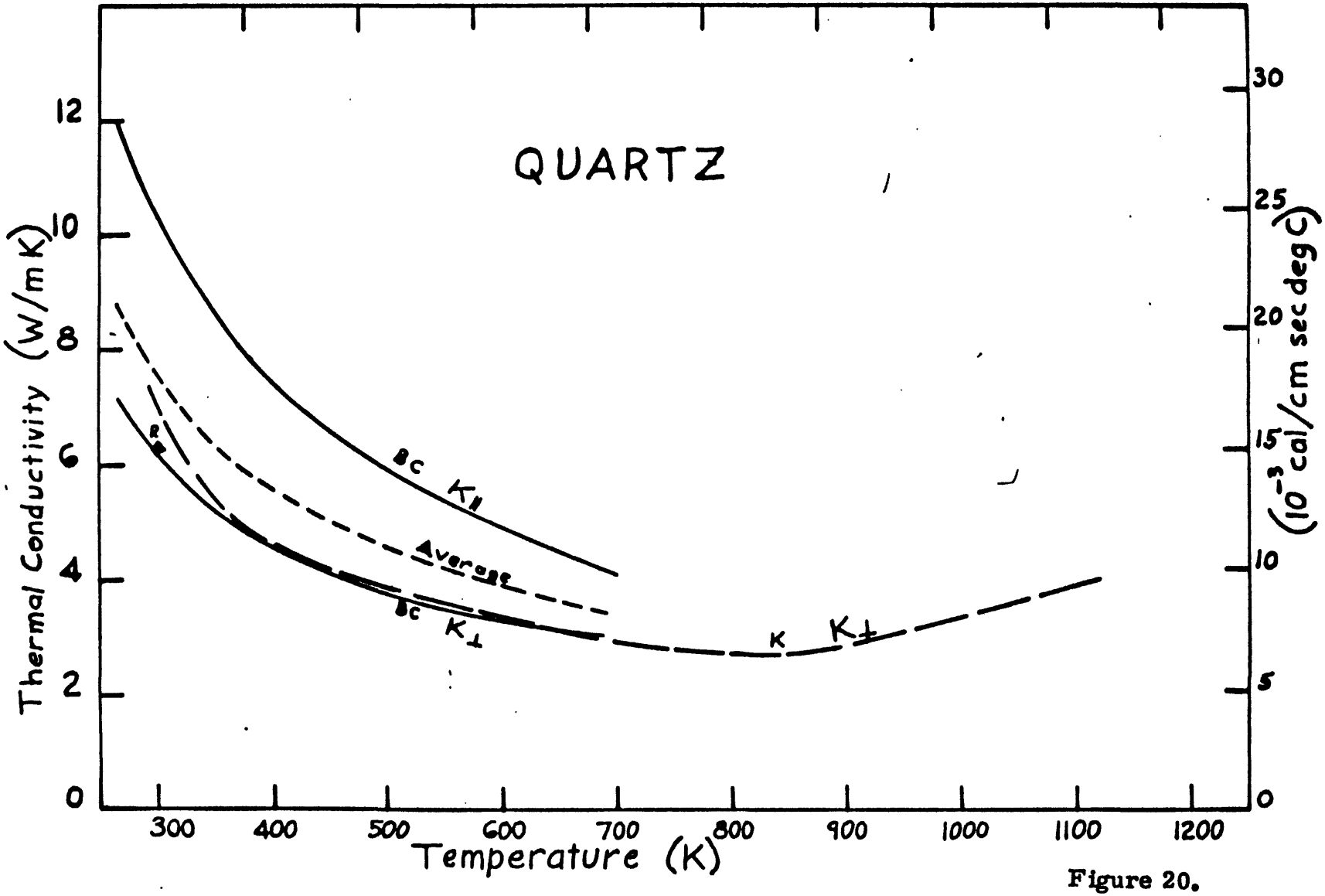

Figure 20.
(Robertson)

and for Figures 15 and 17, the estimates of $\underline{K}$ from γ^2 and as a f ($\underline{T}$) of quartz-bearing rocks depend critically on the content of quartz. The effect of $\underline{T}$ on $\underline{K}$ of single crystal quartz is particularly large at relatively low $\underline{T}$, as shown in Figure 20.

The data for the curves in Figure 20 are from Birch and Clark (1940), marked "BC" and Kanamori et al (1969), marked "K". The symbols "// " and "$\perp$" mean parallel and perpendicular to the C-axis of quartz crystal. The average value shown is calculated by weighting the $\perp$ value by a factor of 2.

Figure 21.

In assessing rock salt beds and domes as repositories for radioactive waste, the temperature coefficient and the pressure coefficient of $\underline{K}$ are important to know. In Figure 21, the curves for single crystal halite at atmospheric pressure from data of Birch and Clark (1940), marked "B-C", and of Schneider (1961), marked "S", show the $\underline{T}$ effect on $\underline{K}$. The curves for Eucken (1911) marked "E", and for McCarthy and Ballard (1960) marked "M-B", are shown to indicate the variation in measurement at 1 bar. The two sets of preliminary results on rocksalt to about 300° C, made for the OWI program by D. D. Smith (written communication, 1976) and by J. G. Moore (written communication, 1977), lie quite near and parallel to the single crystal curve for halite.

The pressure effect on $\underline{K}$ of single crystal halite between - 28° C and + 113°C was measured by Ahlm and Backstrom (1975); curves from their data in Figure 21 are marked "A-B", with the pressure in kb in parentheses. The average pressure coefficient is equal to $+ 3.05 \times 10^{-5}$ bar $^{-1}$, and it applies in the range, 1 bar to 30 kb; this translates to + 3 °/$_o$ /kb, a minor effect on $\underline{K}$ compared to the $\underline{T}$ effect in the near-surface crust of the earth.

The tentative designs of excavations for radioactive waste disposal in salt include placing a back-fill of crushed rocksalt in the canister chambers. The thermal conductivity of such a porous salt aggregation can be estimated by simulating a line of $\underline{K}$ versus γ^2, like that in Figure 4 for limestone, by drawing between the value of $\underline{K}$ at the $\underline{T}$ of interest, taken from Figure 21, and the value for air, K = 0.063 CU. An estimate of the porosity, and solidity, can be made fairly easily. Admittedly, such a figure would be only an approximation, but it should be useful in this application.

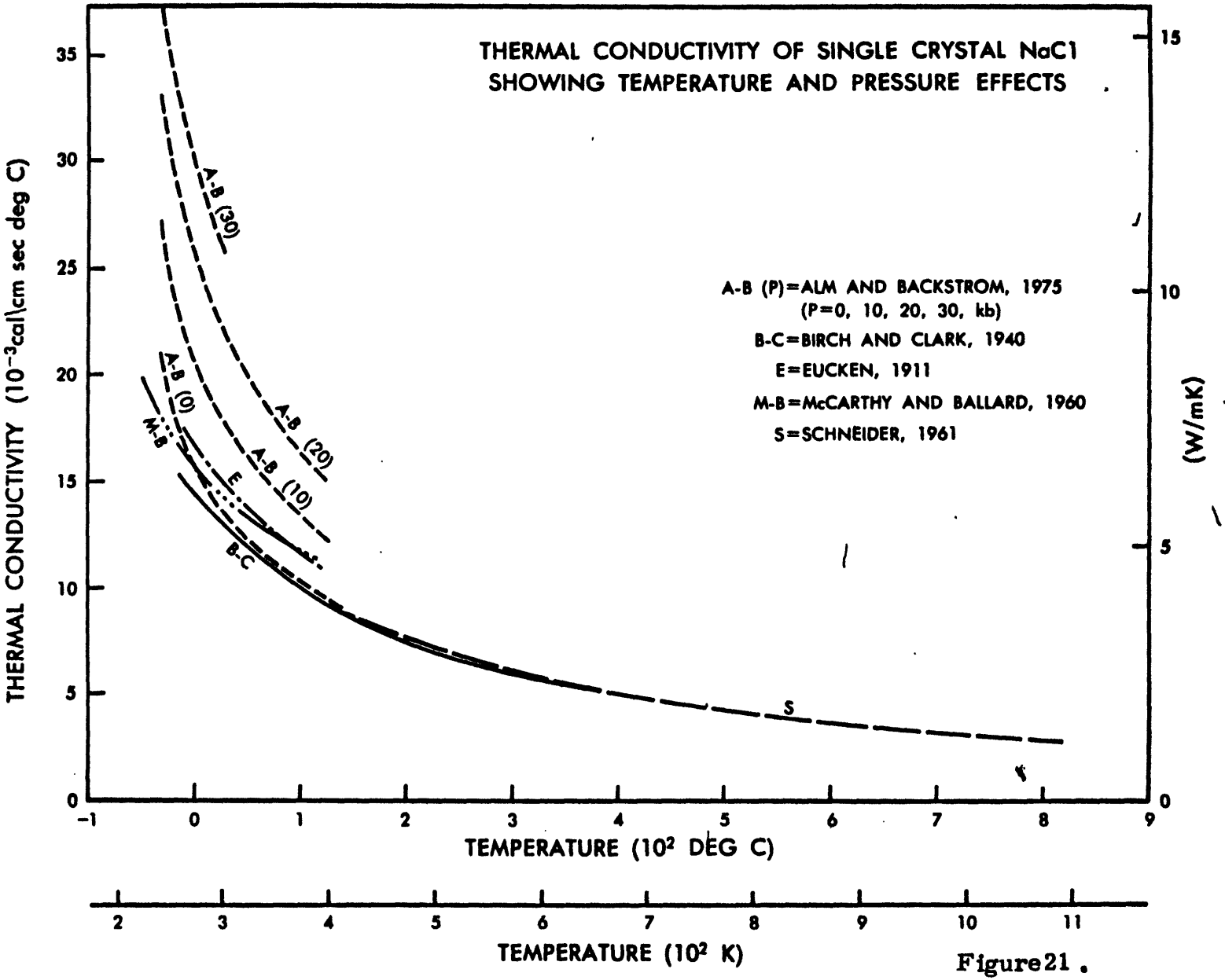

Figure 21.
(Robertson)

References

Adler, D., L. P. Flora, and S. D. Senturia, Electrical conductivity in disordered systems, Solid State Commun., 12, 9-12, 1973.

Alm, O., and Backstrom, G., 1975, Thermal conductivity of NaCl up to 40 k bar and 240-400 K, High Temperatures-High Pressures, v. 7, no. 2, p. 235-239.

Anand, J., Somerton, W. H., and Gomaa, E., 1973, Predicting thermal conductivities of formations from other known properties, Soc. Petroleum Engineers Journal, vol. 13, no. 1, p. 267-273.

Asaad, Yousri., 1955, A study of the thermal conductivity of fluid-bearing porous rocks: University of California, Berkeley, 1955, Ph. D. Thesis, p. 71.

Beck, A. E., and Beck, J. M., 1958: On the measurement of the thermal conductivities of rocks by observations on a divided bar apparatus, American Geophys. Union, Trans., vol. 39, no. 6, pp. 1111-1123.

Beck, A. E., Anglin, F. M., and Sass, J. H., 1971: Analysis of heat flow data-in situ thermal conductivity measurements, Canadian Jour. Earth Sci., vol. 8, no. 1, pp. 1-19.

Benfield, A. E., 1947: A heat flow value for a well in California, Am. Jour. Sci., vol. 245, no. 1, p. 1-18.

Birch, F., and Clark, H., 1940: The thermal conductivity of rocks and its dependence upon temperature and composition, Am. Jour. Sci., vol. 238, nos., 8, 9, pp. 529-635.

Bridgman, P. W., 1924: The thermal conductivity and compressibility of several rocks under high pressure, Amer. Jour. Sci., v. 7, p. 81-102, 1924.

Bullard, E. C., 1939: Heat flow in South Africa, Proc. Roy. Soc. Ser A, no. 955, vol. 173, p. 474-502.

Bullard, E. C., and Niblett, E. R., 1951: Terrestrial heat flow in England, Mon. Not. Roy. Astr. Soc., Geophys. Suppl., vol. 6, no. 4, p. 222-238.

Clark, H., 1941: The effects of simple compression and wetting on the thermal conductivity of rocks, Trans. Amer. Geophy. Union, vol. 22, Part II, p. 543-544.

Coster, H. P., 1947: Terrestrial heat flow in Persia, Mon. Not. Roy. Astr. Soc., Geophys. Suppl. vol. 5, no. 5, pp. 131-145.

Diment, W. H., 1964: Thermal conductivity of serpentinite from Mayaguez, Puerto Rico, and other localities, in, A study of serpentinite, C. A. Burk, (Editor), NAS-NRC Pub. 1188, p. 92-150.

Eucken, A., 1911: Uber die Temperaturabhangigkeit der Warmeleitfahigkeit fester Nichtmetalle, Ann. Physik vol. 34, 185-221.

Greenberg, R. J., and Brace, W. F., 1969: Archie's law for rocks modeled by simple networks, Am. Geophys. Union, Jour. Geophys. Research, vol. 74, no. 8, pp. 2099-2102.

Herrin, E., and Clark, Jr., S. P., 1956: Heat flow in West Texas and Eastern New Mexico, Geophysics, vol. XXI, no. 4, pp. 1087-1099.

Higashi, A., 1952, Thermal conductivity of frozen soil, Hokkaido Univ. Fac. Sci. Jour. pp. 95-106.

Horai, K., 1971: Thermal conductivity of rock-forming minerals, Jour. Geophys. Research, vol. 76, no. 5, pp. 1278-1308.

Hutt, J. R., and Berg, J. Jr., 1968: Thermal and electrical conductivities of sandstone rocks and ocean sediments: Geophysics, vol. 33, no. 3, p. 489-500.

Kanamori, H., Mizutani, H., and Fujii, N., 1969: Method of thermal diffusivity measurement, J. of Physics of the earth, vol. 17, no. 1, p. 43-53.

Kawada, K., 1964: Studies of the thermal state of the earth. The 15th paper: Variation of thermal conductivity of rocks. Part 1. Bull. of the Earthquake Research Institute, vol. 42, p. 631-647.

Kawada, K., 1966, Studies of the thermal state of the earth. The 17th paper: Variation of thermal conductivity of rocks. Part 2, Bull. of the Earthquake Research Institute, vol. 44, p. 1071-1091.

Kersten, M. S., 1949: Thermal properties of soils, Minnesota Univ., Bull. no. 28, vol. 52, no. 21.

King, W., and Simmons, G., 1972: Heat flow near Orlando, Florida and Uvalde, Texas determined from well cuttings, Geothermics, Intl. Jour. Geothermal Res., vol. 1, no. 4, pp. 133-139.

Kunii, D., and Smith, J. M., 1961: Thermal conductivities of porous rocks filled with stagnant fluid, Soc. Petroleum Engineers Jour., vol. 1, no. 1, p. 37-42.

McCarthy, K. A., and Ballard, S. S., 1960: Thermal conductivity of eight halide crystals in the temperature range 220°K to 390°K, J. Appl. Phys., vol. 31, no. 8, p. 1410-1412.

Mirkovich, V. V., 1968, Experimental study relating thermal conductivity to thermal piercing of rocks: Int. J. Rock Mech. Min. Sci. vol. 5, p. 205-218.

Misener, A. D., Thompson, L. G. D. and Uffen, R. J., 1951: Terrestrial heat flow in Ontario and Quebec, Amer. Geophys. Union Trans., v. 32, p. 729-738.

Mossop, S. C., and Gafner, G., 1951: The thermal constants of some rocks from the Orange Free State, Jour., Chem., Metallurgical & Mining Soc., South Africa, vol. 52, no. 4, p. 61-67.

Peck, D. L., Hamilton, M. S., and Shaw, H. R., 1977: Numerical analysis of lava lake cooling models: Part II, Application to Alae Lava Lake, Hawaii, Amer. Jour. Sci., v. 277, p. 415-437.

Penner, E., 1963: Anisotropic thermal conduction in clay sediments, in, International Clay Conference 1963, vol. 1, Intl. Ser. monographs, Earth Sci., vol. 14, edited by T. Rosenqvist and P. Graffe-Petersen, Pergamon Press, N. Y., p. 365-371.

Petrunin, G. I., Yurchak, R. L., and Tkach, G. F., 1971: Temperature conductivity of basalts at temperatures from 300 to 1200°K, Sci. Comm. Fiziko Zemli, no. 2, p. 65-68.

Poole, H. H., 1914, On the thermal conductivity and specific heat of granite and basalt at high temperatures.Phil. Mag. Ser. 6, vol. 27, p. 58-83.

Robertson, E. C., 1959: Physical properties of limestone and dolomite cores from the sandhill well, Wood County, West Virginia, W. Va. Geol. Survey, Morgantown, W. Va., Report of Investigations No. 18, 1959, p. 111-144.

Robertson, E. C., and Peck, D. L., 1974: Thermal conductivity of vesicular basalt from Hawaii, J. Geophys. Res., vol. 79, no. 32, pp. 4875-4888.

Schneider, W. A., 1961, Investigation of the radiative contribution to the thermal conductivity in sodium chloride, dunite and fused quartz, Ph. D. Thesis, Mass. Inst. Tech., June, 1961, 160 p.

Smith, W. O., and Byers, H. G., The thermal conductivity of dry soils of certain of the great soil groups, Soil Sci. Soc. Amer. Proc. 1938, vol. 3, pp. 13-19.

Stephens, D. R., 1963: High temperature thermal conductivity of six rocks, UCRL-7605, 15 p.

Sugawara, A., and Yoshizawa, Y., 1961: An investigation on the thermal conductivity of porous materials and its application to porous rock. Australian J. of Phys., v. 14, no. 4, p. 469-480.

Sugawara, A., and Yoshizawa, Y., 1962: An experimental investigation on the thermal conductivity of consolidated porous materials: J. Appl. Phys., v. 33, p. 3135-3138.

Sukharev, G. M., and Sterlenko, Z. V., 1970: Thermal properties of sandstone saturated distilled water and oil, Teplovie svotstva Peschankov, Nasishchennich Presnoi Vodoi and Neffi, Dokladi Akademii Nauk, SSSR, vol. 194, no. 3, p. 683-685.

Weber, M., 1895: Conductibilite calorifique des roches et des corps mauvais conducteurs, Sciences Physiques et Naturelles Archives, vol. 23, p. 590-591.

Woodside, W. and Messmer, J. H., 1961: Thermal conductivity of porous media. I. Unconsolidated sands, II. Consolidated rocks, Jour. Appl. Physics, vol. 32, no. 9, pp. 1688-1706.

Zierfuss, H., and Vliet, Van Der G., Am. Assoc. Petroleum Geologists Bull., vol. 40, no. 10 (Oct. 1956) pp. 2475-2488, 7 Figs.

Zierfuss, H., 1969: Heat conductivity of some carbonate rocks and clayey sandstones. Amer. Assoc. of Petroleum Geologists Bull. vol. 53, no. 2, p. 251-260.